JOURNAL OF GUIDANCE, CONTROL, AND DYNAMICS
Vol. 29, No. 2, March–April 2006

# Optimization of a Broad Class of Ephemeris Model Earth–Mars Cyclers

Ryan P. Russell*
*Jet Propulsion Laboratory, California Institute of Technology, Pasadena, California 91109*
and
Cesar A. Ocampo†
*University of Texas at Austin, Austin, Texas 78712-1085*

**Recent interest in cycler trajectories has led to the discovery of many new solutions. Most, however, are valid only in a circular-coplanar solar system. The current study presents a method to optimize accurate model cyclers based on simple model solutions and catalogs the results for a broad class of ephemeris model Earth–Mars cyclers. An efficient constrained optimization problem is defined to accommodate long-duration, ballistic, patched conic trajectories. A continuation algorithm is then developed to transition infinitely continuous circular-coplanar solutions to finite-duration accurate ephemeris solutions. Finally, the algorithm is applied to 203 promising circular-coplanar parent cyclers for 21 launch windows each, equaling 4263 cases. In total, there are nine parent cyclers (one of them is the well-known Aldrin cycler) that have at least one finite-duration cycler with a total maneuver requirement of less than 1 m/s over seven full cycles. Additionally, 39 and 74 parent cyclers have at least one launch date with a maneuver requirement of less than 10 and 300 m/s, respectively. Several of the most promising cyclers have consistently low requirements for all launch windows considered. In general, the study demonstrates the broad feasibility for accurate ephemeris cyclers.**

## Introduction

A PLANETARY cycler trajectory is a periodic orbit that shuttles a spaceship indefinitely between two or more planets. Recent interest in developing a cycler-type architecture as a viable alternative to the traditional approach to a human-crewed Mars mission has led to the discovery of many previously unknown Earth–Mars ballistic cycler orbits. However, because of the complexity of the problem, most of the solutions are found in an idealized circular-coplanar model. Of course, this begs the question of their existence in a more accurate model. This problem has been successfully addressed for individual cyclers by a number of researchers; however, the current study seeks to find accurate ephemeris solutions for a broad class of idealized cyclers.

Because the relative geometry of the true solar system is not exactly repeatable, true periodic cycler trajectories do not exist. Thus, quasi-periodic orbits over a finite number of cycles are sought when searching for cycler orbits in an accurate solar system. Although similar in nature, the general problem of finding realistic cyclers is significantly more complicated than the problem of finding cyclers in a circular-coplanar model. The repeat time for the relative geometry of Earth and Mars in the circular-coplanar case is one synodic period, whereas the true model only has an approximate repeat time of seven, or more accurately, 15 synodic periods. The solution space for a 7- or 15-synodic period cycler trajectory is extraordinarily large vs the more reasonable one-, two-, or three-synodic period time frames associated with the circular-coplanar model. A potential 15-synodic period trajectory can contain on the order of 50 legs and as many flybys and powered maneuvers. Reference 1 demonstrates the enormity of the solution space for a simple three-synodic period trajectory using an enumerative approach. Clearly, the same method is not feasible when considering a 15-synodic period (or greater) cycler. The most obvious approach is to use solutions from the simple model as a starting point in the search for realistic cyclers.

Reference 2 gives an overview of the past and current research on simple model cycler trajectories. References 1 and 3 provide detailed summaries of most of the existing documented simple model free-return cycler solutions. In particular, Ref. 1 presents 203 promising solutions with repeat times of three-synodic periods or less. These solutions are representative of a broad class of free-return Earth–Mars cyclers and encompass many of the previously published simple model cyclers such as those from Refs. 3–7. This study seeks to find and optimize ephemeris model versions of each of these 203 promising simple model cyclers.

Previous efforts to identify realistic cyclers have focused on the circular-coplanar model, very accurate high-fidelity models, and several models in between. References 8–10 use an idealized resonance between Earth, Mars, and Venus, including both the circular-coplanar model and a model accounting for the mean eccentricities and inclinations of the planets. In the case of the Earth and Mars, Ref. 8 documents several ballistic cyclers in each model with general repeat times of four synodic periods or greater. Reference 11 extends the VISIT cycler concept to include a 20-year propagation using an accurate ephemeris. Reference 7 demonstrates the real-world feasibility of the Aldrin cycler, also known as an escalator orbit, by minimizing required maneuvers in an accurate multiconic optimizer. Reference 12 gives a low-thrust version of the same cycler optimized in an accurate ephemeris model. Reference 5 shows a seven-cycle propagation of a near-ballistic two-synodic period cycler. Reference 13 gives hundreds of launch opportunities and associated characteristics for the S1L1 cycler using a true ephemeris. Note the S1L1 indicates the cycler is constructed of a short-period 1-revolution Earth–Earth transfer, followed by a long-period 1-revolution Earth–Earth transfer. The ballistic S1L1 solutions with favorable characteristics were obtained using a continuation method that slowly increases the complexity of the solar-system model until finally a true ephemeris is used. References 12 and 14 present true ephemeris versions of powered Earth–Mars cyclers using low-thrust and a direct optimization technique. Although still in an idealized model, Ref. 15 demonstrates the preliminary design of solar-sail

Received 25 September 2004; revision received 6 December 2004; accepted for publication 7 December 2004. 

*Engineer, M/S 301-140L, 4800 Oak Grove Drive; Ryan.Russell@jpl.nasa.gov. Member AIAA.
†Associate Professor, C0600, Department of Aerospace Engineering, 1 University Station. Member AIAA.

cyclers using optimal control theory. References 16–18 summarize much of the previous work and propose several metrics associated with Earth–Mars cycler and hybrid cycler concepts when evaluating the overall design of a powered cycler architecture. The advantages and disadvantages of ballistic, low-thrust, and impulsive thrust cyclers and hybrid cyclers are discussed.

In general, the basic structure of solutions associated with circular-coplanar models are reflected in the analogous solutions using an accurate ephemeris. The nonrepeating geometry of the true model, however, does have a significant, often unpredictable, effect on the important characteristics associated with cyclers, such as the interplanetary transit times and hyperbolic excess velocities at Earth and Mars. As demonstrated in Ref. 13, a given parent cycler can produce an unlimited number of accurate ephemeris cyclers, each with varying characteristics that depend on the desired launch date and propagation time.

The purpose of this study is to develop a robust method that is capable of finding true ephemeris counterparts to the circular-coplanar parent cyclers. The goal is of course to identify purely ballistic cyclers, meaning all maneuvers are achievable with flybys only. However, because many of the existing circular-coplanar ballistic (or near-ballistic) solutions already require flybys that are near (or violate) the minimum altitude boundary of 200 km, it is not expected that each simple solution has ballistic counterparts in a true ephemeris model. Thus, it is necessary to include the possibility for propulsive maneuvers. The solution method is selected based on efficiency and robustness because it must accommodate over 200 parent cyclers, each with a variety of launch dates. As a result, the selected method is direct and optimizes impulsive maneuvers only. Further optimization of any given cycler is considered beyond the scope of this study, although it is encouraged as future work. Examples include higher-fidelity gravity models, alternative impulsive optimization, low-thrust capability, and indirect methods.

In total, 21 different launch windows are considered for each of the 203 parent cyclers presented in Ref. 1, requiring 4263 cases. Total powered maneuver requirements are presented for each launch window for all one- and two-synodic period parent cyclers and a select group of three-synodic period parent cyclers. Seventy-four parent cyclers are found to have at least one launch window requiring total maneuvers less than 300 m/s over the seven-cycle duration, and 39 of those solutions require less than 10 m/s. Reproducible trajectories are archived in Ref. 19 for the minimum $\Delta v$ launch date for each of the selected 74 parent cyclers.

Because Ref. 1 includes most of the useful and previously published free-return Earth–Mars cyclers, this study is a broad and robust survey of the true ephemeris cyclers of the same class. The method presented proves to be a reliable preliminary design tool for accurate ephemeris cyclers. It demonstrates the existence of hundreds of previously unpublished ballistic or very near-ballistic accurate ephemeris cyclers. Although the general pattern is assumed to be repeatable, it is emphasized that the cycler trajectories presented include total $\Delta v$ requirements to maintain seven cycles only. The injection requirements and maneuvers necessary to patch consecutive seven-cycle segments are not included in the analysis.

## Problem Definition and Assumptions

Final trajectories are sought that use a realistic ephemeris file, Jet Propulsion Laboratory's DE405,[20] to obtain the positions and velocities of the planets. The mean obliquity[21] of the ecliptic is used to rotate all vectors so that they are referenced to the mean equinox and ecliptic plane of J2000. As long as the final trajectories use an ephemeris file, it is completely valid to use intermediate solutions that propagate the planets using Kepler's equation. The motion of the cycler spacecraft is assumed to be governed by the sun only; thus, Keplerian propagation is sufficient. Also, consecutive trajectories legs are patched using an instantaneous patched conic flyby with a minimum altitude of 200 km. However, unlike the assumptions in Refs. 1 and 3, flybys at Mars are included. In the circular-coplanar model, these were ignored because of the low mass of Mars, but more importantly, so that cyclers could be constructed using Earth–Earth free returns only. It is expected that this extra degree of freedom might alleviate some of the problems associated with the nonideal orbits of Earth and Mars. All flybys are modeled with the assumption that they occur instantaneously and the radius of the planet's sphere of influence is zero.

The inertial positions of Earth and Mars approximately repeat every 15 years, and several previous studies have used this as a baseline to determine the duration of a true cycler propagation.[5,7,13,14] Earlier studies, however, assumed (with more accuracy) that the basic repeat time of the true solar system is 32 years.[8–10]

A more detailed look at the relative geometries of the true orbits of Earth and Mars shows that there are several approximate repeat times worth considering. It is desirable to find in the true solar system an $X$:$Y$ resonance between Earth and Mars, meaning the Earth makes exactly $X$ revolutions for every $Y$ Mars revolutions, where $X$ and $Y$ should be as close to integers as possible. If a resonance existed where $X$ and $Y$ were exactly integers, then the relative geometry of Earth and Mars would be exactly repeatable (under the assumption that the sun is the only attracting body). Of course perfect Earth–Mars resonances in the true solar system do not exist. Table 1 lists several pertinent Earth–Mars resonances based on their mean periods.[21]

Also, the total duration for the propagation must be an integer multiple of the repeat time of the parent cycler in the circular-coplanar model. Table 2 gives the total duration for a given number of cycles for cyclers with repeat times of one, two, three, and four synodic periods, respectively.

Each entry of Table 2 is compared with each of the first numbers in the second column of Table 1. The bold entries are suggested as reasonable total durations. Certain bold entries are better than others as indicated by how close to integers their values are and the magnitude of the associated residuals from Table 1. For example, for three-synodic period cyclers, 32.03 is very near 32, and the 32:17 resonance has one of the smallest residuals listed; therefore, five cycles appears to be a prudent choice for the total duration of an accurate ephemeris version of a three-synodic period cycler. Note that Table 1 only includes near resonances that have corresponding

**Table 1 Earth–Mars resonances**

| Accurate $X$:$Y$ resonance (Earth revs: Mars revs) | Approximate $X$:$Y$ resonance (Earth revs: Mars revs) | \|Residual\| (revs) |
|---|---|---|
| 15.000: 7.9755 | 15:8 | 0.0245 |
| 17.000: 9.0389 | 17:9 | 0.0389 |
| 30.000: 15.9510 | 30:16 | 0.0490 |
| 32.000: 17.0144 | 32:17 | 0.0144 |
| 34.000: 18.0778 | 34:18 | 0.0778 |
| 45.000: 23.9265 | 45:24 | 0.0735 |
| 47.000: 24.9899 | 47:25 | 0.0101 |
| 60.000: 31.9020 | 60:32 | 0.0980 |
| 64.000: 34.0288 | 64:34 | 0.0288 |
| 77.000: 40.9409 | 77:41 | 0.0591 |
| 94.000: 49.9798 | 94:50 | 0.0202 |

**Table 2 Integer multiples of circular-coplanar cycler repeat times**

| Number of cycles | 1-synodic period, yr | 2-synodic period, yr | 3-synodic period, yr | 4-synodic period, yr |
|---|---|---|---|---|
| 1 | 2.14 | 4.27 | 6.41 | 8.54 |
| 2 | 4.27 | 8.54 | 12.81 | **17.08** |
| 3 | 6.41 | 12.81 | 19.22 | 25.62 |
| 4 | 8.54 | **17.08** | 25.62 | **34.17** |
| 5 | 10.68 | 21.35 | **32.03** | 42.71 |
| 6 | 12.81 | 25.62 | 38.44 | 51.25 |
| 7 | **14.95** | **29.90** | **44.84** | **59.79** |
| 8 | 17.08 | **34.17** | 51.25 | 68.33 |
| 9 | 19.22 | 38.44 | 57.66 | **76.87** |
| 10 | 21.35 | 42.71 | **64.06** | 85.42 |
| 11 | 23.49 | **46.98** | 70.47 | **93.96** |
| 12 | 25.62 | 51.25 | 76.87 | 102.50 |
| 13 | 27.76 | 55.52 | 83.28 | 111.04 |
| 14 | **29.90** | 59.79 | 89.69 | 119.58 |
| 15 | **32.03** | **64.06** | 96.09 | 128.12 |

bold entries in Table 2. For example, the resonance 49.0000:26.0533 is not included in Table 1 because there is no cycler repeat time near 49 years as indicated in Table 2.

Although it is expected that the general structure and pattern of a 32-year propagation is repeatable, it is not guaranteed. Even if the total time is constrained to be exactly 32 years, the resonance is not perfect, and furthermore, no considerations have been made for feasibility of the flybys that would eventually patch multiple 32-year segments. Therefore, it is assumed that nontrivial powered maneuvers might be necessary to ultimately patch the multiple cycle segments. Thus, when considering how to choose the total duration of a multiple cycle segment, it is desirable to include as many cycles as possible.

The method developed in this study favors efficiency over performance in some instances because of the large number of cases that need evaluation. Therefore, all cyclers will be propagated for seven cycles, as it is the only row in Table 1 with all bold entries. Additionally, this choice is consistent with previous studies.[5,7,13,14] For further optimization of a particular cycler, it is recommended to use 15 cycles (32 years) for a one-synodic period cycler, 11 cycles (47 years) for a two-synodic period cycler, either 5 or 10 cycles (32 or 64 years) for a three-synodic period cycler, and seven or 11 cycles (60 or 94 years) for a four-synodic period cycler.

As discussed in Ref. 1, only one short Earth–Mars or Mars–Earth transit is guaranteed per cycle. Thus, it is decided to search for accurate ephemeris solutions for cyclers with repeat times of three synodic periods or less. Only outbound cyclers, or cyclers with short Earth–Mars legs, will be considered. Minor modifications are necessary to evaluate inbound cyclers, and it is reasonable to expect similar results.

In summary, the main objective is to develop an efficient and robust method to optimize seven continuous cycles of a given circular-coplanar parent cycler using patched conic two-body motion between true ephemeris planet locations. In general, it is loosely assumed that the basic structure of the seven-cycle sequence is repeatable indefinitely. It is emphasized, however, that no explicit constraint is enforced to ensure the repeatability of the seven cycles. Yet, the constraint is loosely and implicitly enforced because of the generally repeating inertial positions of Earth and Mars every seven cycles. Based on this extra degree of freedom, it is reasonable to expect that certain finite-duration ephemeris cyclers will have improved characteristics compared to their simple-model counterparts.

## Solution Method

There are many different approaches to consider when searching for true ephemeris solutions. This section will discuss the advantages and disadvantages of several options and explain in detail the selected method.

### Continuation Method

The basic idea of a continuation[22] method, also referred to as imbedding or a homotopy method, is to solve a sequence of several subproblems, where the fidelity of the model in question is increased for each subproblem until the desired level of complexity is achieved. The solution to each subproblem becomes the initial guess for each successive subproblem. A continuation method is ideal for the Earth–Mars cycler problem because solutions to the first subproblem (circular-coplanar case) are readily available from previous studies. However, one of the shortcomings of a continuation method is that solutions to each subproblem must exist in order to continue along the path. The solution to the last subproblem is the only one of interest, yet it might not be possible to get there even if a solution exists because the problem can become infeasible at one or more of the intermediate steps.

In most cases, the gap between the circular-coplanar model and the accurate ephemeris model prohibits an immediate jump to the latter. Therefore, the continuation method is deemed most appropriate, and other considerations are made to address its apparent shortcomings.

### Nonanalytic Solutions

Several attempts were made to use the analytic solutions for the interplanetary transfers presented in Refs. 2 and 23. These include the full-revolution return solutions, half-revolution return solutions, and the generic (not necessarily return) transfers. These solutions are extremely fast, accurate, and relatively straightforward to implement. However, each case requires at least two integer-valued inputs. Each circular-coplanar cycler has a unique set of integer identifiers as specified in the formal cycler nomenclature.[2] These integer values fix the structure of each leg of the trajectory. However, as the complexity of the model moves toward the accurate case, it is feasible and very probable that the trajectory as a whole could benefit from minor changes in this structure. For instance, a short-period one-revolution transfer from Mars to Earth that exists in the circular-coplanar case might cease to exist when the launch and arrival dates become free parameters and move away from their original values. Of course, there is always a transfer that connects two points, but changing the value of the integer inputs (such as number of revolutions and indicating if it is a short-period or long-period solution) is a difficult if not insurmountable obstacle when dealing with a gradient-based optimizer.

Solving the transfers analytically with a defined fixed structure works very well for cyclers with favorable turning angle requirements, such as the S1L1 cycler.[13] However, because the method developed for this study must be capable of optimizing any circular-coplanar cycler regardless of its characteristics, the nonanalytic approach is a better choice. In this method, a specific transfer is found by numerically searching for the spacecraft velocity vector that leads to an intercept of the desired planet. This approach eliminates the integer programming problem, and the solution structure is free to morph as necessary. A major benefit to this approach is the relative ease of gradient calculations. Although tedious, partial derivatives of the final states with respect to the unknown velocities and times can be calculated analytically. The same calculations become much more difficult when Lambert's equation is part of the solution process. The analytic derivatives are discussed in a later section.

### Gradient Method

For the problem at hand, a gradient method is favored over a Monte Carlo or genetic-algorithm (GA)[24] approach based on convergence properties and computational requirements. There are two major advantages of a genetic algorithm: a GA searches a global solution space and requires no gradient information. For individual cyclers, some success is achieved using a genetic algorithm[‡] and the analytic transfer solutions. This is certainly a valid approach to trajectory optimization[25,26]; however, it is not considered practical for this study because it is not efficient when considering all the cases and launch dates that need consideration.

Although gradient methods give rise to local solutions, the fact that the solutions in the circular-coplanar case are ballistic gives confidence that the analogous solutions in the accurate model will be good locally optimal solutions if not globally optimal. Two standard sequential-quadratic-programming packages are used to optimize the free parameters. The first package is VF13 from the Harwell Subroutine Library.[§] This code works well with cyclers with favorable turning characteristics, but often fails when the constraints become infeasible. The second package is the SNOPT (Sparse Nonlinear Optimizer) driver from the Stanford Business Software, Inc.[27,¶] SNOPT proves to be more robust for purposes of this study. It has a "non-linear elastic mode" that automatically minimizes a weighted sum of the absolute values of the constraint violations (in addition to an existing objective if any) when the constraints become infeasible. This feature provides robustness to the system because the

[‡]Data available online at http://cuaerospace.com/carroll/ga.html [cited 26 May 2004].

[§]Data available online at http://www.cse.clrc.ac.uk/nag/hsl [cited 25 May 2004].

[¶]Data available online at http://www.sbsi-sol-optimize.com/asp/sol_product_snopt.htm [cited 25 May 2004].

algorithm continues to search for a "good solution" even if the optimality conditions are not satisfied or the constraints cannot be met. The continuation method can therefore continue "walking" toward the accurate ephemeris model even if favorable solutions disappear along the path. Details regarding the SNOPT input and the constraint and free parameter choices are in later sections.

**Multiple Shooting Method**

Reference 22 gives a detailed overview of direct multiple shooting methods in the context of other optimization techniques. This section discusses the benefits of multiple shooting methods regarding accurate ephemeris cycler optimization and gives a detailed explanation of the specifically developed method.

The long-duration trajectories associated with accurate ephemeris cycler propagation lend to a multiple shooting approach. If each leg of a multiple-decade patched trajectory is numerically dependent on the final conditions of the previous leg, very small adjustments to the initial conditions of the first leg will lead to highly erratic and nonlinear perturbations at the end of the long trajectory. To avoid the large sensitivities and cumulative numerical errors, a multiple shooting approach defines each leg of a patched trajectory to be completely independent from all other legs.

Specific to the current problem, the seven parameters chosen to completely define each leg are the initial planet, final planet, initial time, final time, and the three components of the initial planet-referenced spacecraft velocity. Except for the specification of the initial and final planets, each of the stated parameters is unknown and free to be optimized. Thus, there are $5n$ unknowns, where $n$ is the number of legs for a particular cycler propagation. A diagram is given in Fig. 1.

The spacecraft initial position is fixed to the planet's initial position, and a planet's position and velocity is uniquely a function of time only via an ephemeris file. The ephemeris can be as accurate as possible, or it can be based on any set of fictional or mean orbital elements referenced to J2000, depending on the desired solar-system model complexity. The sequence of planets remains fixed during the optimization procedure and is selected initially based on multiple cycles of the parent circular-coplanar cycler.

Because each leg is independent, multiple shooting methods require boundary constraints to enforce continuity between the segments. Thus, there are $n-1$ scalar time constraints that directly result from using a multiple shooting approach. Although extra constraints require additional gradient calculations, an added benefit of a multiple shooting method is the favorable structure of the associated gradient matrix, also known as the Jacobian. Again, because each leg is independent, any unknown variable affects only the constraints associated with one leg. Therefore the Jacobian, in general, is expected to be sparse with block matrices along the diagonal. This feature contributed to the selection of SNOPT[**] as the primary optimizer because it was designed explicitly for large sparse problems with many active constraints.

A second benefit of SNOPT is its favorable handling of linear constraints. The time constraint that enforces continuity is $t_{f(i)} = t_{0(i+1)}$. This is a simple linear constraint that SNOPT easily solves during each major iteration of the optimization process. Therefore, disconnecting the times and enforcing a simple linear constraint gives the tremendous benefit of a sparse Jacobian, yet for all practical purposes the constraint is nonexistent because SNOPT solves it completely during every iteration. This is a significant benefit in terms of the computational cost and accuracy of determining the Jacobian, a topic covered in a later section.

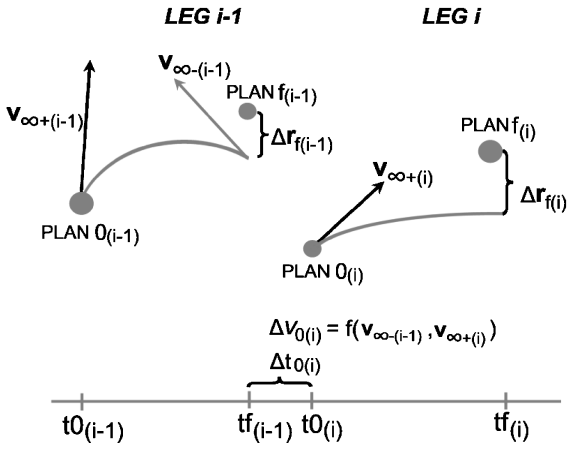


**Fig. 1 Trajectory leg diagram.**

**Ballistic Flybys with Powered Maneuvers at the Sphere of Influence**

A ballistic gravity-assisted flyby is capable of rotating a spacecraft's planet-centered velocity as described in detail in Ref. 23. The magnitude, however, is constrained to be equal before and after the flyby. A second inequality constraint places an upper bound on the angle of rotation based on the flyby speed at the sphere of influence, the gravitational parameter of the flyby body, and the minimum acceptable flyby radius. These two constraints are given in Eqs. (1) and (2). They are enforced at each of the $n-1$ flybys for a trajectory with $n$ legs.

$$\left|\boldsymbol{v}_{\infty-(i-1)}\right| = \left|\boldsymbol{v}_{\infty+(i)}\right| \tag{1}$$

$$\omega_{\text{req}} \leq \omega_{\text{avail}} \tag{2}$$

where

$$\omega_{\text{req}} = \cos^{-1}\left[\frac{\boldsymbol{v}_{\infty-(i-1)}^{\top}\boldsymbol{v}_{\infty+(i)}}{v_{\infty-(i-1)}\,v_{\infty+(i)}}\right] \tag{3}$$

$$\omega_{\text{avail}} = 2\sin^{-1}\left(\frac{\mu_{\text{plan}}}{\mu_{\text{plan}} + r_{p\,\min}\,v_{\infty\,\text{small}}^2}\right) \tag{4}$$

The problem as stated is a nonlinear root finding problem with $5n$ unknowns, $3n+2(n-1)$ equality constraints and $(n-1)$ inequality constraints. It is not an explicit optimization problem because there is no defined objective function. However, as mentioned in the preceding section, if all of the constraints cannot be met, SNOPT automatically enters an "elastic mode" that minimizes the constraint infeasibilities.

One approach to avoid constraint infeasibilities is to introduce four additional unknowns per leg (an intermediate time and three components of a $\Delta\boldsymbol{v}$) and attempt to minimize an explicit objective function defined to be the sum of the magnitudes of all of the intermediate maneuvers. Although this method is valid and might yield more favorable trajectories, it is prohibitive in the current problem because it almost doubles the dimension of the parameter vector.

A second more efficient approach is to take advantage of the elastic mode of SNOPT and redefine the constraints, if possible, to directly measure the powered $\Delta v$ necessary to make each flyby feasible. In this approach, the equality and inequality constraints given in Eqs. (1) and (2) are replaced by one conditional equality constraint given by Eq. (5):

$$\Delta v_{0(i)} = \begin{cases} \left|v_{\infty+(i)} - v_{\infty-(i-1)}\right| & \text{if} \quad \omega_{\text{req}} \leq \omega_{\text{avail}} \\ \sqrt{v_{\infty+(i)}^2 + v_{\infty-(i-1)}^2 - 2v_{\infty+(i)}v_{\infty-(i-1)}\cos(\omega_{\text{req}} - \omega_{\text{avail}})} & \text{if} \quad \omega_{\text{req}} > \omega_{\text{avail}} \end{cases} \tag{5}$$

[**]Data available online at http://www.sbsi-sol-optimize.com/asp/sol_product_snopt.htm [cited 25 May 2004].

**Table 3 Summary of parameters and constraints[a,b]**

| Parameter | Number | Constraint | Number | Type |
|---|---|---|---|---|
| $\boldsymbol{v}_{\infty+(i)}$ | $3n$ | $\boldsymbol{r}_{f(i)} = \boldsymbol{r}_{f\text{plan}(i)}$ | $3n$ | Nonlinear equality |
| $t_{0(i)}$ | $n$ | $t_{f(i-1)} = t_{0(i)}$ | $n-1$ | Linear equality |
| $t_{f(i)}$ | $n$ | $\Delta v_{(i)} = 0$ | $n-1$ | Nonlinear equality |

[a] $i$ indicates the $i$th leg, $n$ = number of legs.
[b] $5n$ total parameters and $5n-2$ total constraints.

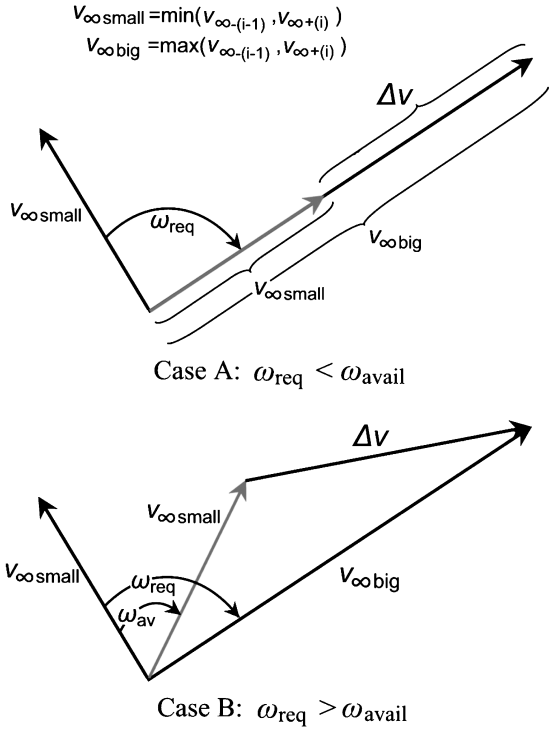


**Fig. 2 Powered $\Delta v$ required at the SOI of a flyby.**

This approach does not increase the number of unknowns, eliminates the inequality constraints, and does not introduce an explicit performance index. A summary of the parameters and newly defined constraints is given in Table 3.

A diagram explaining the origin of Eq. (5) is given in Fig. 2. Given the unknowns associated with any two successive legs, the trajectories are propagated according to Fig. 1. At the end of the $(i-1)$st leg, $\boldsymbol{v}_{\infty-(i-1)}$ can be deduced, and $\boldsymbol{v}_{\infty+(i)}$ is simply three of the given unknowns. Their magnitudes can be calculated and are not necessarily equal. The required turning angle is found via the definition of a dot product and is given by Eq. (3). The maximum available turning angle is derived from basic properties of hyperbolic trajectories and is given in Eq. (4). It is desirable to use the smallest value of $v_\infty$ because it is inversely related to the available turning angle. If $v_{\infty-(i-1)} > v_{\infty+(i)}$, then the powered maneuver should occur before the flyby; otherwise, it should occur afterwards. All maneuvers take place during heliocentric flight just outside the planet's sphere of influence (SOI), which is currently modeled with a zero radius. A powered maneuver during the hyperbolic phase of a flyby is considered too risky and is beyond the scope of this study despite the acknowledged potential for fuel savings.

In case A of Fig. 2, the required turning angle can be achieved using a gravity-assisted flyby alone, while the powered maneuver is simply to account for the difference in magnitudes. In case B, the flyby provides the maximum turning angle available, meaning the flyby has a periapse altitude of 200 km. To optimize the effects of the flyby, it is performed in the plane that contains $\boldsymbol{v}_{\infty-(i-1)}$ and $\boldsymbol{v}_{\infty+(i)}$. The remaining scalar $\Delta v$ is calculated using the law of cosines and is given in Eq. (5).

### Analytic Gradient Calculations

The need to calculate partial derivatives is a common problem encountered in astrodynamics and trajectory optimization. More generally, almost all root-finding or optimization methods require some form of gradient information relating sensitivity of the constraints and the objective with respect to the free parameters.

Numerical approximation is a brute force method that is easy to implement and is sufficient for most applications. However, the selection of a perturbation size is a tuning parameter that requires significant attention in order to achieve the most accurate gradient possible.[28] Numerical derivatives are also computationally expensive. In general, each forward- or central-differenced derivative requires one or two additional constraint function calls, respectively. This run-time penalty is particularly unfavorable for the current application because thousands of different cycler trajectories require optimization.

An alternative approach is to calculate the partial derivatives analytically. This can be a very difficult and tedious task depending on the complexity of the constraints and their relationships to each parameter. The expressions must be checked and rederived each time a constraint or parameter is introduced or redefined in a particular problem. However, once implemented, analytic gradients are the most accurate available and in most cases are significantly faster than approximating the derivatives numerically.[29] Analytic derivatives are much better suited for the current application because the structure of the problem is fixed.

In this section, analytic expressions for the nonzero partial derivatives of the constraints with respect to the unknowns for the defined accurate ephemeris cycler problem are derived. This gradient matrix, or the Jacobian, consists of $5n-2$ rows and $5n$ columns because from Table 3 there are $5n-2$ constraints and $5n$ unknowns. This totals $25n^2-10n$ entries; thus, for a propagation of an accurate ephemeris cycler with 35 legs there are 30,275 Jacobian entries. Fortunately a multiple shooting approach is used, and most of these entries are zero.

In general, there are five scalar constraints associated with each leg as summarized in Table 3. The first leg is the only exception because there is no prior leg to patch. The only nonzero partial derivatives of $\boldsymbol{C}_i$, the constraints associated with a particular leg, with respect to $\boldsymbol{U}_i$, the unknowns associated with a particular leg, are given in Eq. (6):

$$\frac{\partial \boldsymbol{C}_1}{\partial \boldsymbol{U}_1} = \begin{bmatrix} \dfrac{\partial \Delta \boldsymbol{r}_{f(1)}}{\partial \boldsymbol{v}_{\infty+(1)}} & \dfrac{\partial \Delta \boldsymbol{r}_{f(1)}}{\partial t_{0(1)}} & \dfrac{\partial \Delta \boldsymbol{r}_{f(1)}}{\partial t_{f(1)}} \end{bmatrix}$$

$$\underset{i=2\to n}{\frac{\partial \boldsymbol{C}_i}{\partial \boldsymbol{U}_i}} = \begin{bmatrix} \dfrac{\partial \Delta \boldsymbol{r}_{f(i)}}{\partial \boldsymbol{v}_{\infty+(i)}} & \dfrac{\partial \Delta \boldsymbol{r}_{f(i)}}{\partial t_{0(i)}} & \dfrac{\partial \Delta \boldsymbol{r}_{f(i)}}{\partial t_{f(i)}} \\ \boldsymbol{0}_{1\times 3} & \dfrac{\partial \Delta t_{0(i)}}{\partial t_{0(i)}} & 0 \\ \dfrac{\partial \Delta v_{0(i)}}{\partial \boldsymbol{v}_{\infty+(i)}} & 0 & 0 \end{bmatrix}$$

$$\underset{i=2\to n}{\frac{\partial \boldsymbol{C}_i}{\partial \boldsymbol{U}_{i-1}}} = \begin{bmatrix} \boldsymbol{0}_{3\times 3} & \boldsymbol{0}_{3\times 1} & \boldsymbol{0}_{3\times 1} \\ \boldsymbol{0}_{1\times 3} & 0 & \dfrac{\partial \Delta t_{0(i)}}{\partial t_{f(i-1)}} \\ \dfrac{\partial \Delta v_{0(i)}}{\partial \boldsymbol{v}_{\infty+(i-1)}} & \dfrac{\partial \Delta v_{0(i)}}{\partial t_{0(i-1)}} & \dfrac{\partial \Delta v_{0(i)}}{\partial t_{f(i-1)}} \end{bmatrix} \tag{6}$$

The final structure of the full Jacobian is given here:

$$\begin{bmatrix} \left(\frac{\partial \boldsymbol{C}_1}{\partial \boldsymbol{U}_1}\right)_{3\times 5} & & & & & \\ \left(\frac{\partial \boldsymbol{C}_2}{\partial \boldsymbol{U}_1}\right)_{5\times 5} & \left(\frac{\partial \boldsymbol{C}_2}{\partial \boldsymbol{U}_2}\right)_{5\times 5} & & & 0 & \\ & \left(\frac{\partial \boldsymbol{C}_3}{\partial \boldsymbol{U}_2}\right)_{5\times 5} & \left(\frac{\partial \boldsymbol{C}_3}{\partial \boldsymbol{U}_3}\right)_{5\times 5} & & & \\ \cdots & \cdots & \cdots & \cdots & \cdots & \cdots \\ & 0 & & \left(\frac{\partial \boldsymbol{C}_{n-1}}{\partial \boldsymbol{U}_{n-2}}\right)_{5\times 5} & \left(\frac{\partial \boldsymbol{C}_{n-1}}{\partial \boldsymbol{U}_{n-1}}\right)_{5\times 5} & \\ & & & & \left(\frac{\partial \boldsymbol{C}_n}{\partial \boldsymbol{U}_{n-1}}\right)_{5\times 5} & \left(\frac{\partial \boldsymbol{C}_n}{\partial \boldsymbol{U}_n}\right)_{5\times 5} \end{bmatrix}_{(5n-2)\times(5n)}$$

Equation (6) is derived intuitively by a close evaluation of Fig. 1 and the relationships between the constraints and parameters given in Table 3. The partial derivatives can be simplified as follows:

$$\frac{\partial \Delta \boldsymbol{r}_{f(i)}}{\partial \boldsymbol{v}_{\infty+(i)}} = \frac{\partial\left[\boldsymbol{r}_{f(i)} - \boldsymbol{r}_{\mathrm{PLAN}f(i)}\right]}{\partial \boldsymbol{v}_{\infty+(i)}} = \frac{\partial\left[\boldsymbol{r}_{f(i)}\right]}{\partial \boldsymbol{v}_{\infty+(i)}}$$

$$= \frac{\partial \boldsymbol{r}_{f(i)}}{\partial \boldsymbol{v}_{0(i)}}\frac{\partial \boldsymbol{v}_{0(i)}}{\partial \boldsymbol{v}_{\infty+(i)}} = \frac{\partial \boldsymbol{r}_{f(i)}}{\partial \boldsymbol{v}_{0(i)}}\boldsymbol{I}_{3\times 3} = \frac{\partial \boldsymbol{r}_{f(i)}}{\partial \boldsymbol{v}_{0(i)}}$$

$$\frac{\partial \Delta \boldsymbol{r}_{f(i)}}{\partial t_{0(i)}} = \frac{\partial\left[\boldsymbol{r}_{f(i)} - \boldsymbol{r}_{\mathrm{PLAN}f(i)}\right]}{\partial t_{0(i)}} = \frac{\partial \boldsymbol{r}_{f(i)}}{\partial t_{0(i)}}$$

$$\frac{\partial \Delta \boldsymbol{r}_{f(i)}}{\partial t_{f(i)}} = \frac{\partial\left[\boldsymbol{r}_{f(i)} - \boldsymbol{r}_{\mathrm{PLAN}f(i)}\right]}{\partial t_{f(i)}} = \boldsymbol{v}_{f(i)} - \boldsymbol{v}_{\mathrm{PLAN}f(i)} = \boldsymbol{v}_{\infty-(i)}$$

$$\frac{\partial \Delta t_{0(i)}}{\partial t_{f(i-1)}} = \frac{\partial\left[t_{0(i)} - t_{f(i-1)}\right]}{\partial t_{f(i-1)}} = -1$$

$$\frac{\partial \Delta t_{0(i)}}{\partial t_{0(i)}} = \frac{\partial\left[t_{0(i)} - t_{f(i-1)}\right]}{\partial t_{0(i)}} = 1$$

$$\frac{\partial \Delta v_{0(i)}}{\partial \boldsymbol{v}_{\infty+(i-1)}} = \frac{\partial \Delta v_{0(i)}}{\partial \boldsymbol{v}_{\infty-(i-1)}}\frac{\partial \boldsymbol{v}_{\infty-(i-1)}}{\partial \boldsymbol{v}_{\infty+(i-1)}} = \frac{\partial \Delta v_{0(i)}}{\partial \boldsymbol{v}_{\infty-(i-1)}}\frac{\partial \boldsymbol{v}_{\infty-(i-1)}}{\partial \boldsymbol{v}_{0(i-1)}}$$

$$= \frac{\partial \Delta v_{0(i)}}{\partial \boldsymbol{v}_{\infty-(i-1)}}\frac{\partial \boldsymbol{v}_{f(i-1)}}{\partial \boldsymbol{v}_{0(i-1)}}$$

$$\frac{\partial \Delta v_{0(i)}}{\partial t_{0(i-1)}} = \frac{\partial \Delta v_{0(i)}}{\partial \boldsymbol{v}_{\infty-(i-1)}}\frac{\partial \boldsymbol{v}_{\infty-(i-1)}}{\partial t_{0(i-1)}}$$

$$= \frac{\partial \Delta v_{0(i)}}{\partial \boldsymbol{v}_{\infty-(i-1)}}\frac{\partial\left[\boldsymbol{v}_{f(i-1)} - \boldsymbol{v}_{\mathrm{PLAN}f(i-1)}\right]}{\partial t_{0(i-1)}} = \frac{\partial \Delta v_{0(i)}}{\partial \boldsymbol{v}_{\infty-(i-1)}}\frac{\partial \boldsymbol{v}_{f(i-1)}}{\partial t_{0(i-1)}}$$

$$\frac{\partial \Delta v_{0(i)}}{\partial t_{f(i-1)}} = \frac{\partial \Delta v_{0(i)}}{\partial \boldsymbol{v}_{\infty-(i-1)}}\frac{\partial \boldsymbol{v}_{\infty-(i-1)}}{\partial t_{f(i-1)}}$$

$$= \frac{\partial \Delta v_{0(i)}}{\partial \boldsymbol{v}_{\infty-(i-1)}}\left[\boldsymbol{a}_{f(i-1)} - \boldsymbol{a}_{\mathrm{PLAN}f(i-1)}\right]$$

Thus, Eq. (6) becomes

$$\frac{\partial \boldsymbol{C}_1}{\partial \boldsymbol{U}_1} = \begin{bmatrix} \frac{\partial \boldsymbol{r}_{f(1)}}{\partial \boldsymbol{v}_{0(1)}} & \frac{\partial \boldsymbol{r}_{f(1)}}{\partial t_{0(1)}} & \boldsymbol{v}_{\infty-(1)} \end{bmatrix}$$

$$\underset{i=2\to n}{\frac{\partial \boldsymbol{C}_i}{\partial \boldsymbol{U}_i}} = \begin{bmatrix} \frac{\partial \boldsymbol{r}_{f(i)}}{\partial \boldsymbol{v}_{0(i)}} & \frac{\partial \boldsymbol{r}_{f(i)}}{\partial t_{0(i)}} & \boldsymbol{v}_{\infty-(i)} \\ \boldsymbol{0}_{1\times 3} & 1 & 0 \\ \frac{\partial \Delta v_{0(i)}}{\partial \boldsymbol{v}_{\infty+(i)}} & 0 & 0 \end{bmatrix}$$

$$\underset{i=2\to n}{\frac{\partial \boldsymbol{C}_i}{\partial \boldsymbol{U}_{i-1}}} = \begin{bmatrix} \boldsymbol{0}_{3\times 3} & \boldsymbol{0}_{3\times 1} & \boldsymbol{0}_{3\times 1} \\ \boldsymbol{0}_{1\times 3} & 0 & -1 \\ \boldsymbol{A}\frac{\partial \boldsymbol{v}_{f(i-1)}}{\partial \boldsymbol{v}_{0(i-1)}} & \boldsymbol{A}\frac{\partial \boldsymbol{v}_{f(i-1)}}{\partial t_{0(i-1)}} & \boldsymbol{A}\left[\boldsymbol{a}_{f(i-1)} - \boldsymbol{a}_{\mathrm{PLAN}f(i-1)}\right] \end{bmatrix} \tag{7}$$

where

$$\boldsymbol{A} = \frac{\partial \Delta v_{0(i)}}{\partial \boldsymbol{v}_{\infty-(i-1)}}$$

The remaining few derivatives are separated into three general categories. The corresponding partials are derived in the following three sections.

*Partials of the Final State with Respect to the Initial State*[30]

In general, the spacecraft state, $\boldsymbol{x} = [\boldsymbol{r}\ \ \boldsymbol{v}]^\top$, is governed by a first-order differential equation:

$$\frac{\mathrm{d}\boldsymbol{x}(t)}{\mathrm{d}t} = \boldsymbol{f}[\boldsymbol{x}(t), t]$$

Taking the partial derivative with respect to the state at an initial time gives

$$\frac{\partial}{\partial \boldsymbol{x}(t_0)}\frac{\mathrm{d}\boldsymbol{x}(t)}{\mathrm{d}t} = \frac{\partial \boldsymbol{f}[\boldsymbol{x}(t), t]}{\partial \boldsymbol{x}(t_0)}$$

$$\frac{\mathrm{d}}{\mathrm{d}t}\frac{\partial \boldsymbol{x}(t)}{\partial \boldsymbol{x}(t_0)} = \frac{\partial \boldsymbol{f}[\boldsymbol{x}(t), t]}{\partial \boldsymbol{x}(t)}\frac{\partial \boldsymbol{x}(t)}{\partial \boldsymbol{x}(t_0)}$$

and can be rewritten as

$$\frac{\mathrm{d}\boldsymbol{\Phi}(t, t_0)}{\mathrm{d}t} = \frac{\partial \boldsymbol{f}[\boldsymbol{x}(t), t]}{\partial \boldsymbol{x}(t)}\boldsymbol{\Phi}(t, t_0) \tag{8}$$

where

$$\boldsymbol{\Phi}(t, t_0) = \frac{\partial \boldsymbol{x}(t)}{\partial \boldsymbol{x}(t_0)}$$

The partial derivative of the state at a final time with respect to the state at an initial time is therefore $\boldsymbol{\Phi}(t, t_0)$ by definition. The matrix $\boldsymbol{\Phi}$ is often referred to as the state transition matrix and can be obtained by numerically integrating Eq. (8) with the initial condition of $\boldsymbol{\Phi}(t_0, t_0) = \boldsymbol{I}_{6\times 6}$. This is true for any force model that is a function of the state and time only.

For simple Keplerian motion, if the state is expressed as the classic orbital elements $\boldsymbol{\alpha} = [a\ \ e\ \ i\ \ \omega\ \ \Omega\ \ M]^\top$, instead of position and velocity $\boldsymbol{x}$, then the state transition matrix is analytic and has the same entries as the identity matrix except

$$\phi_{\alpha 6,1}(t, t_0) = -3(t - t_0)\sqrt{\mu/a^5}\Big/2$$

Thus, for Keplerian orbits the partial of the final Cartesian state with respect to the initial Cartesian state can be calculated

analytically without integrating the state transition matrix numerically. This expression is given in Eq. (9):

$$\frac{\partial \boldsymbol{x}(t)}{\partial \boldsymbol{x}(t_0)} = \frac{\partial \boldsymbol{x}(t)}{\partial \boldsymbol{\alpha}(t)} \frac{\partial \boldsymbol{\alpha}(t)}{\partial \boldsymbol{\alpha}(t_0)} \frac{\partial \boldsymbol{\alpha}(t_0)}{\partial \boldsymbol{x}(t_0)}$$

$$= \frac{\partial \boldsymbol{x}(t)}{\partial \boldsymbol{\alpha}(t)} \boldsymbol{\Phi}_{\alpha}(t, t_0) \frac{\partial \boldsymbol{\alpha}(t_0)}{\partial \boldsymbol{x}(t_0)} \tag{9}$$

Reference 30 gives detailed derivations for the partials of the Cartesian coordinates with respect to the classic orbital elements and the inverses, respectively. Both partial derivative matrices have entries with singularities when eccentricity or inclination is zero. This is a dilemma for the current application because every cycler has at least one Earth to Earth generic leg that takes place in the ecliptic, and most half-revolution returns have small if not zero eccentricities.

As a result, an unconventional set of orbital elements $\boldsymbol{\beta}$ can be defined such that the partials are well behaved at low eccentricities and inclinations. References 31 and 32 define two such sets. The latter nonsingular set is defined as

$$\boldsymbol{\beta} = [a \quad e\sin(\Omega+\omega) \quad e\cos(\Omega+\omega)\sin(i/2)\sin(\Omega) \quad \sin(i/2)\cos(\Omega) \quad \Omega+\omega+M]^{\top}$$

Thus, the final form of Eq. (9) is

$$\frac{\partial \boldsymbol{x}(t)}{\partial \boldsymbol{x}(t_0)} = \frac{\partial \boldsymbol{x}(t)}{\partial \boldsymbol{\beta}(t_0)} \frac{\partial \boldsymbol{\beta}(t_0)}{\partial \boldsymbol{x}(t_0)} \tag{10}$$

where the first term on the right side of the equation has the state transition matrix for the new orbital element set embedded and is found directly with the equations given in Ref. 32. The second term on the right is found by inverting the partial of $\boldsymbol{x}(t)$ with respect to $\boldsymbol{\beta}(t_0)$ when $t = t_0$.

Note that there are several typographical errors in the equations in Appendix 1 of Ref. 32; however, the FORTRAN code in Appendix 2 of Ref. 32 is correct. The equations for $\partial \boldsymbol{x}/\partial \boldsymbol{\alpha}$ and $\partial \boldsymbol{x}/\partial \boldsymbol{\beta}$ found in Refs. 30 and 32, respectively, are well documented and require several pages of calculations. For brevity, they are not rewritten here.

*Partials of the Final State with Respect to the Initial Time*

For the current problem as defined in Table 3, the state of a spacecraft on a given leg is a function only of the of the initial state and the time elapsed since $t_0$. The initial position is a function of $t_0$ only, and the initial velocity is a function of $t_0$ and $\boldsymbol{v}_{\infty+}$ only.

$$\boldsymbol{x}(t) = f[\boldsymbol{r}_0(t_0), \boldsymbol{v}_0(t_0, \boldsymbol{v}_{\infty+}), t - t_0]$$

The partial of $\boldsymbol{x}$ with respect to $t_0$ is

$$\frac{\partial \boldsymbol{x}(t)}{\partial t_0} = \frac{\partial \boldsymbol{x}(t)}{\partial \boldsymbol{r}_0} \frac{\partial \boldsymbol{r}_0}{\partial t_0} + \frac{\partial \boldsymbol{x}(t)}{\partial \boldsymbol{v}_0} \frac{\partial \boldsymbol{v}_0}{\partial t_0} + \frac{\partial \boldsymbol{x}(t)}{\partial (t-t_0)} \frac{\partial (t-t_0)}{\partial t_0} \tag{11}$$

where

$$\frac{\partial \boldsymbol{r}_0}{\partial t_0} = \boldsymbol{v}_{\mathrm{PLAN}\,0}, \qquad \frac{\partial \boldsymbol{v}_0}{\partial t_0} = \boldsymbol{a}_{\mathrm{PLAN}\,0}, \qquad \text{and} \qquad \frac{\partial (t-t_0)}{\partial t_0} = -1$$

$$\frac{\partial \boldsymbol{x}(t)}{\partial (t-t_0)} = \frac{\partial \boldsymbol{x}(t)}{\partial M(t)} \frac{\partial M(t)}{\partial (t-t_0)} \tag{12}$$

where

$$M(t) = M_0 + \sqrt{\mu/a^3}(t-t_0)$$

Equation (12) is true because the only orbital element affected by $t - t_0$ is the mean anomaly $M$. The term $\partial \boldsymbol{x}(t)/\partial M(t)$ is given in Sec. 7.1.2 of Ref. 30 and also is identical to $\partial \boldsymbol{x}(t)/\partial \beta_6(t_0)$ from Eq. (10), which is obtained using the equations in Ref. 32.

The final form of the partial derivative of the final state with respect to the initial time is given in Eq. (13):

$$\frac{\partial \boldsymbol{x}(t_f)}{\partial t_0} = \frac{\partial \boldsymbol{x}(t_f)}{\partial \boldsymbol{r}_0} \boldsymbol{v}_{\mathrm{PLAN}\,0} + \frac{\partial \boldsymbol{x}(t_f)}{\partial \boldsymbol{v}_0} \boldsymbol{a}_{\mathrm{PLAN}\,0} - \frac{\partial \boldsymbol{x}(t_f)}{\partial M(t)} \sqrt{\frac{\mu}{a^3}} \tag{13}$$

*Partials of the Powered $\Delta v$ Constraint*

The only two terms from Eq. (7) that remain unknown are

$$\frac{\partial \Delta v_{0(i)}}{\partial \boldsymbol{v}_{\infty-(i-1)}} \qquad \text{and} \qquad \frac{\partial \Delta v_{0(i)}}{\partial \boldsymbol{v}_{\infty+(i)}}$$

The expression for $\Delta v_{0(i)}$ is given in Eq. (5). Dropping the $i$ subscripts, these partial derivatives can be written as

$$\frac{\partial \Delta v_0}{\partial \boldsymbol{v}_{\infty\pm}} =$$

$$\begin{cases} \dfrac{|v_{\infty+} - v_{\infty-}|}{v_{\infty+} - v_{\infty-}} \left( \pm \dfrac{\partial v_{\infty\pm}}{\partial \boldsymbol{v}_{\infty\pm}} \right) & \text{if} \quad \omega_{\mathrm{req}} \le \omega_{\mathrm{avail}} \\ \dfrac{1}{\Delta v_0} \left\{ v_{\infty\pm} \dfrac{\partial v_{\infty\pm}}{\partial \boldsymbol{v}_{\infty\pm}} - v_{\infty\mp} \left[ \dfrac{\partial v_{\infty\pm}}{\partial \boldsymbol{v}_{\infty\pm}} \cos(\omega_{\mathrm{req}} - \omega_{\mathrm{avail}}) \right.\right. \\ \left.\left. - v_{\infty\pm} \sin(\omega_{\mathrm{req}} - \omega_{\mathrm{avail}}) \left( \dfrac{\partial \omega_{\mathrm{req}}}{\partial \boldsymbol{v}_{\infty\pm}} - \dfrac{\partial \omega_{\mathrm{avail}}}{\partial \boldsymbol{v}_{\infty\pm}} \right) \right] \right\} & \text{if} \quad \omega_{\mathrm{req}} > \omega_{\mathrm{avail}} \end{cases}$$

where

$$v_{\infty\pm} = \sqrt{\boldsymbol{v}_{\infty\pm}^{\top} \boldsymbol{v}_{\infty\pm}}, \qquad \frac{\partial v_{\infty\pm}}{\partial \boldsymbol{v}_{\infty\pm}} = \frac{\boldsymbol{v}_{\infty\pm}^{\top}}{v_{\infty\pm}}$$

Differentiating Eqs. (3) and (4) and dropping the $i$ subscripts gives

$$\frac{\partial \omega_{\mathrm{avail}}}{\partial \boldsymbol{v}_{\infty\,\mathrm{small}}} = 4\boldsymbol{v}_{\infty\,\mathrm{small}}^{\top} \left[ \frac{-\mu_{\mathrm{plan}} r_{p\,\mathrm{min}}}{\left(\mu_{\mathrm{plan}} + r_{p\,\mathrm{min}} v_{\infty\,\mathrm{small}}^2\right)^2} \right] \Bigg/ \sqrt{1 - \left( \frac{\mu_{\mathrm{plan}}}{\mu_{\mathrm{plan}} + r_{p\,\mathrm{min}} v_{\infty\,\mathrm{small}}^2} \right)^2}$$

$$\frac{\partial \omega_{\mathrm{avail}}}{\partial \boldsymbol{v}_{\infty\,\mathrm{big}}} = 0$$

$$\frac{\partial \omega_{\mathrm{req}}}{\partial \boldsymbol{v}_{\infty\pm}} = -\left[ \frac{\boldsymbol{v}_{\infty\mp}}{v_{\infty\mp}} \left( \frac{\boldsymbol{I}_{3\times 3}}{v_{\infty\pm}} - \frac{\boldsymbol{v}_{\infty\pm} \boldsymbol{v}_{\infty\pm}^{\top}}{v_{\infty\pm}^3} \right) \right] \Bigg/ \sqrt{1 - \left( \frac{\boldsymbol{v}_{\infty-}^{\top} \boldsymbol{v}_{\infty+}}{v_{\infty-} v_{\infty+}} \right)^2}$$

where

$$\boldsymbol{v}_{\infty\,\mathrm{small}} = \begin{cases} \boldsymbol{v}_{\infty-} & \text{if} \quad v_{\infty-} \le v_{\infty+} \\ \boldsymbol{v}_{\infty+} & \text{if} \quad v_{\infty-} > v_{\infty+} \end{cases}$$

$$r_{p\,\mathrm{min\ Earth}} = 6578.0\,\mathrm{km}, \qquad r_{p\,\mathrm{min\ Mars}} = 3598.5\,\mathrm{km}$$

Note, the equations that have variables with $\pm$ or $\mp$ have two valid interpretations: one form with each variable evaluated with top sign and a second form with each variable evaluated with the bottom sign.

**Constraint Infeasibilities and Postprocessing Considerations**

As stated in Table 3, all legs of the patched trajectory have one associated vector constraint, and all legs except the first have two associated scalar constraints. If the current set of unknowns is in a region where all of the constraints cannot be satisfied, SNOPT enters an elastic mode that seeks to reduce the constraint infeasibilities. The linear time continuity constraints are always feasible and easily satisfied, and no explicit objective is defined. Thus, the elastic mode is "equivalent to minimizing the sum of the nonlinear constraint violations."[††] When SNOPT enters this mode, the new composite

[††]Data available online at http://www.sbsi-sol-optimize.com/asp/sol_product_snopt.htm [cited 25 May 2004].

objective becomes

$$J = \sum_{\substack{i=1\to n \\ \Delta v_{0(1)}=0}} \left(\Delta v_{0(i)} + \left|\Delta r_{xf(i)}\right| + \left|\Delta r_{yf(i)}\right| + \left|\Delta r_{zf(i)}\right|\right) \quad (14)$$

The final solution is therefore not guaranteed to intercept the desired planet. However, a final flyable trajectory must, at a minimum, have position continuity between each leg.

One approach to reduce the residuals is to simply weight the position constraints (and associated derivatives) in the original formulation inside the constraint definition. This is equivalent to adjusting the composite objective function to

$$J = \sum_{\substack{i=1\to n \\ \Delta v_{0(1)}=0}} \left[\Delta v_{0(i)} + W\left(\left|\Delta r_{xf(i)}\right| + \left|\Delta r_{yf(i)}\right| + \left|\Delta r_{zf(i)}\right|\right)\right] \quad (15)$$

For sufficiently large values of $W$, the solution will effectively ignore the $\Delta v$ requirements, focusing only on the position violations, and vice versa for sufficiently small values. Clearly, this parameter requires tuning to identify what value leads to the best solutions.

A second method to achieve position continuity is to postprocess the final trajectory by adding intermediate maneuvers to remove the residuals entirely. These can be independently optimized, but the final magnitudes must be added to the total cycler cost.

After much trial and error, a hybrid of both approaches is selected. A variety of test trajectories are optimized using a range of weight factors $W$. The final solutions, each with various magnitudes for the position residuals, are postprocessed for continuity, and the total cost is evaluated to choose the best weight factor.

Canonical variables are used for calculations in this study such that the gravitational parameter of the sun is unity. Thus, the magnitudes of positions and velocities are similar. Each component of Eq. (15) is therefore expected to be of equal magnitude when $W$ is on the order of one. After many trade studies, the best value for $W$ appeared to be exactly one, and this value was used for the thousands of subsequent runs. The serendipitous best value of one is indicative of the benefits of using canonical units for astrodynamic applications.

To reduce the effect of the postprocessed intermediate maneuvers on the overall fuel costs, the time of each maneuver is independently optimized over the course of the given leg. This one-dimensional optimization problem is globally solved with a simple grid search over 100 equally spaced intervals, paying close attention to avoid $n\pi$ transfer angles.

As a whole, trajectories are evaluated based on the total accumulated $\Delta v$ following the postprocessing. Although the intermediate maneuvers are not included in the original optimization problem, this hybrid approach gives good results and benefits tremendously from the increase in speed vs including the postprocessed maneuvers in the original problem formulation.

The general solution method described in this section is used to optimize over 200 different parent cycler trajectories, each with 21 different launch windows. As a result, it is designed to be robust, efficient, and capable of accommodating all types of long-duration patched ballistic transfers. Presumably, any number of existing ballistic interplanetary trajectory optimization codes[33–35] could be used to further optimize any of the solutions. In the initial stages of this study, COPERNICUS[35] was used for trade studies to identify promising options for the constraint and parameter definitions. COPERNICUS is a high-fidelity general trajectory optimization package currently under development at the University of Texas at Austin.

#### Algorithm Description

As described in earlier sections, a continuation approach is selected to walk solutions from the circular-coplanar model to an accurate ephemeris model. There are many potential paths to consider when transitioning a solution from a simple model to a more accurate one. Similar to the method used in Ref. 13, the approach that generally gives the best results consists of three major steps. These are outlined as follows:

0) Circular-coplanar model (mean values for Earth and Mars at J2000 for $a$, $\Omega$, $\omega$, and $v$; but $e = i = 0$)

**Table 4 Mean elements at J2000[21]**

| Classic orbital element | Earth | Mars |
|---|---|---|
| $a$ (au) | $1.00000101812E{+}00$ | $1.52367934749E{+}00$ |
| $e$ | $1.67086171540E{-}02$ | $9.34006199474E{-}02$ |
| $i$, deg | $0.00000000000E{+}00$ | $1.84972647778E{+}00$ |
| $\Omega$, deg | $0.00000000000E{+}00$ | $4.95655237028E{+}01$ |
| $\omega$, deg | $1.02937348083E{+}02$ | $2.86494710278E{+}02$ |
| $v$, deg | $-2.47089957222E{+}00$ | $1.93730406472E{+}01$ |

1) Use continuation method to "walk" toward mean eccentricities for Earth and Mars with *nstep* equally spaced "steps"

2) Use continuation method to "walk" toward mean inclinations for Earth and Mars with *nstep* equally spaced "steps"

3) Make one final "step" from the now mean orbital element model directly to the accurate ephemeris.

It is very important to fix the initial values of $a$, $\Omega$, $\omega$, and $v$ for Earth and Mars to their respective mean values at J2000; otherwise, the model changes too rapidly. Table 4 gives the mean values for the orbital elements of Mars and Earth at J2000.[21]

The algorithm that describes the process is as follows:

FOR *ParentCycler* = 1 to 203
  FOR *LaunchWindow* = 1 to 21
    1) Set Earth and Mars orbital elements to the mean values at J2000
    2) Set Earth and Mars inclination and eccentricity to zero
    3) Propagate simple model from J2000 forward *LaunchWindow* synodic periods.
    4) INPUT the beginning phase angle for current simple model *ParentCycler*
    5) Propagate simple model forward in time until desired phase angle achieved
    6) Record epoch time
    7) INPUT seven cycles of the simple model *ParentCycler* beginning at the epoch time.
    FOR *steploop* = 1 to 6
      1) $nstep = 3^{(steploop-1)}$ (gives *nstep* values of 1, 3, 9, 27, 81, 243)
      2) "WALK" mean eccentricities with *nstep* steps (each step is 1 run of SNOPT)
      3) "WALK" mean inclinations with *nstep* steps (each step is 1 run of SNOPT)
      4) "STEP" to the true ephemeris model (this is 1 run of SNOPT)
      5) Store the total $\Delta v$, the full trajectory characteristics, and the current value of *nstep*
    END *steploop* loop
    8) Of all *nstep* runs, keep the best solution for current *ParentCycler* and *LaunchWindow*
    9) POST-PROCESS this best solution
      1) Optimize times during each leg for intermediate $\Delta v$ to enforce position continuity
      2) Add each intermediate $\Delta v$ to overall cycler $\Delta v$
    10) Write to file the final true eph. sol. for current *ParentCycler* and *LaunchWindow*
  END *LaunchWindow* loop
END *ParentCycler* loop

Analogous ephemeris solutions are sought for each circular-coplanar parent cycler in 21 independent runs, each associated with a different launch window. The launch windows have units of synodic periods after J2000. Thus, a cycler with an associated *LaunchWindow* value of $i$ will have an original epoch time in between $i$ and $i+1$ synodic periods after J2000. Twenty-one is chosen to observe three complete cycles of the approximate seven synodic period repeat time of the true inertial positions of Earth and Mars.

Trade studies are done using different values of *nstep*, or the number of continuation steps used to walk the solution to the accurate ephemeris. The results are inconsistent, meaning the *nstep* value that leads to the best solution varies depending on the parent cycler and launch window. To account for this tuning necessity, each parent cycler and launch window is independently walked using several

different number of steps. Several other loops can be added to consider other tuning variables such as input values to SNOPT or the $\Delta v$ weighting scalar $W$, as discussed in the prior section. However, these tuning loops significantly increase the run time of the algorithm and only provide marginal solution improvement, depending on the specific tuning variable. Therefore, the default input tuning values for SNOPT are generally left unchanged for the final runs.

If the algorithm as stated is modified such that the *nstep* loop only runs once with a value of $nstep = 5$, a value found to be an excellent compromise between efficiency and performance, then the total run time on a 3.2-GHz processor is approximately one day (roughly three days on a 1-GHz processor). The code was written in FORTAN and compiled with a flag to optimize for speed. Roughly, a 50% increase in solution performance can be achieved if the full algorithm is run including the *nstep* loop. However, the increase in performance comes at substantial cost. The full run time is approximately four days running continuously on 15 computers with an average processor speed of 2 GHz (roughly 120 days on a 1-GHz processor). The results of the full run are presented in the next section.

## Results

A full run of the algorithm presented earlier requires the evaluation of 203 parent cyclers, each with 21 different launch dates.

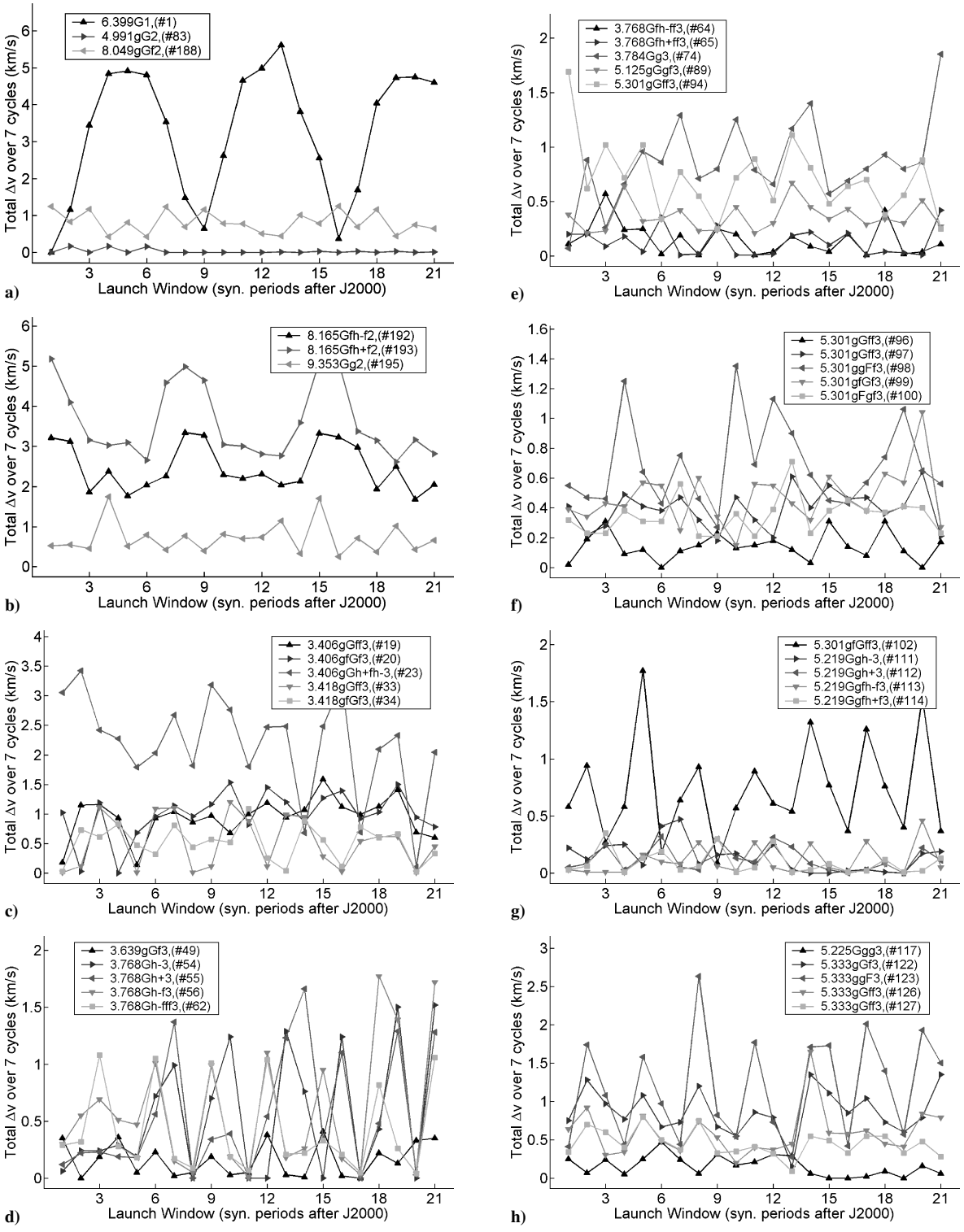


**Fig. 3 Total $\Delta v$ for optimized ephemeris cyclers: Part I.**

Each parent cycler and launch window pair is then walked to a true ephemeris model six different times with *nstep* values of 1, 3, 9, 27, 81, and 243, respectively. The *nstep* values are chosen somewhat arbitrarily to be powers of three, where the primary goal is to efficiently sample a full range of values. In total, the SNOPT driver is called $(203) \times (21) \times [2(1+3+9+27+81+243)+1]$ times equaling 3,107,727 calls. The values inside the bracket account for the number of steps taken for eccentricity, inclination, and finally the last step to the true ephemeris model.

The lowest total $\Delta v$ solution for each *ParentCycler–LaunchWindow* pair is written to a file. This includes $(203) \times (21)$ or 4263 full reproducible trajectories varying from 15 to 49 legs. Obviously, the full details of each trajectory cannot feasibly be archived in this document. However, a summary of the total $\Delta v$ required for the full seven-cycle propagation is presented for a selected set of parent cyclers in Figs. 3 and 4.

Total $\Delta v$ values are presented for each launch window for 77 of the 203 parent cyclers evaluated. All one- and two-synodic period parent cyclers, regardless of the solution characteristics, are included in the results. All three-synodic period parent cyclers with at least one launch date with a total $\Delta v$ requirement of 300 m/s or less are also included.

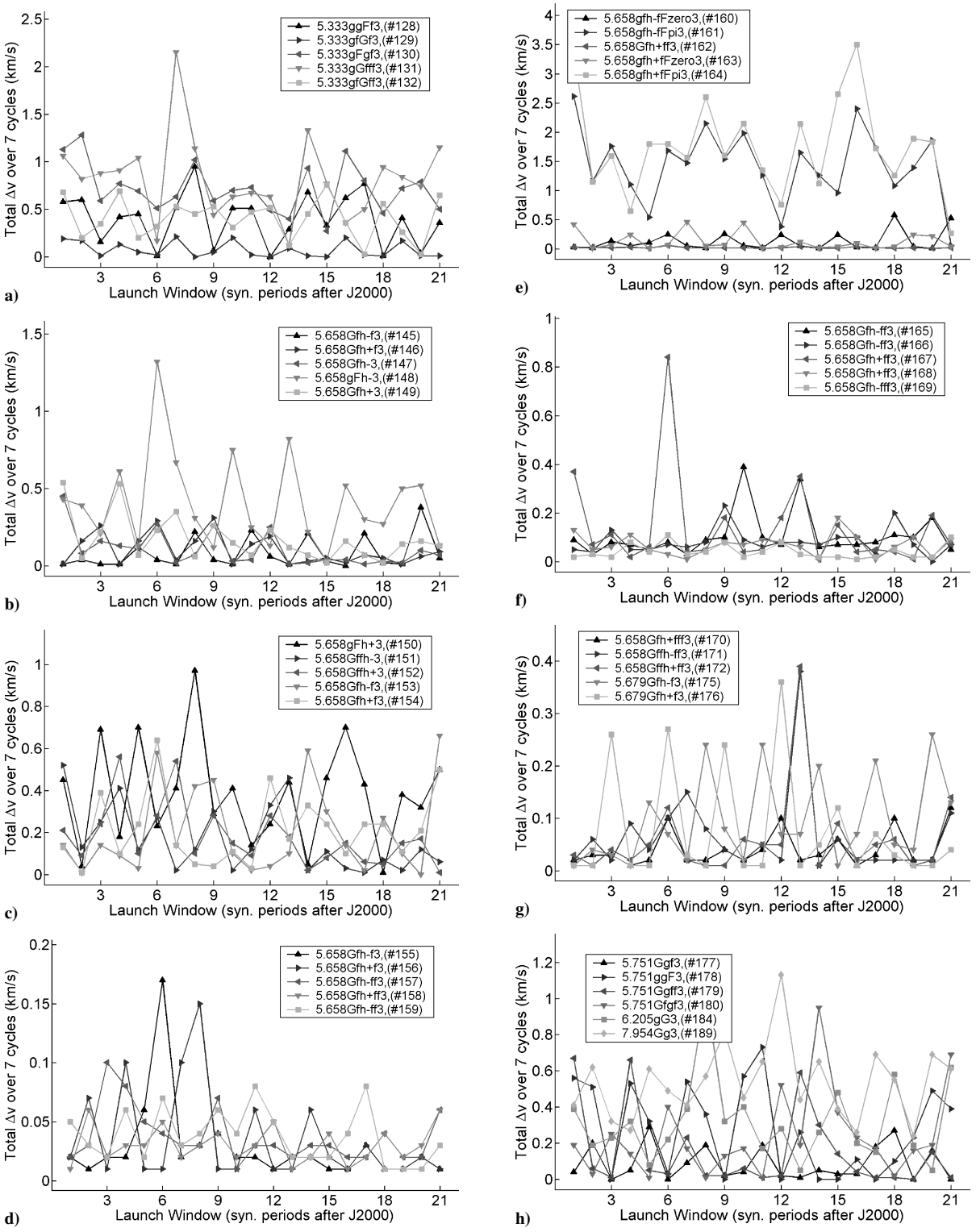


**Fig. 4 Total $\Delta v$ for optimized ephemeris cyclers: Part II.**

The one- and two-synodic period parent cyclers are plotted together in Fig. 3a. In total, one one-synodic period parent cycler and five two-synodic period parent cyclers are evaluated. The remaining 71 parent cyclers have a three-synodic period simple model repeat time. These are sorted according to their simple model Earth hyperbolic excess speed and specific sequence of free returns.

The shorthand names for each of the parent cyclers are extended to uniquely differentiate each one from those presented in Ref. 1. The first number is the simple model Earth hyperbolic excess speed. The last number prior to the # is the repeat time of the cycler in synodic periods. The sequence of letters in between indicate the type and order of the free returns, which is an abbreviation of the formal cycler nomenclature developed in Ref. 2. The + or − following each h indicates whether the half-revolution return is above or below the ecliptic plane. A capital letter indicates the Earth–Mars leg occurs on this Earth–Earth free return. If the capital letter is an F, a zero or $\pi$ follows to indicate the longitude of the full-revolution return, noting that it must be zero or $\pi$ to exist in the ecliptic plane. The unique number that follows the # is included for ease of reference to a particular parent cycler.

In general, the results are promising. There are 9, 39, and 74 parent cyclers that have at least one launch date that requires a total $\Delta v$ of less than 1, 10, and 300 m/s, respectively. Several of the most promising cyclers have consistently low $\Delta v$ requirements for all launch windows considered. Most notable is cycler 4.991gG2(#83) as seen in Fig. 3a. Also known as the S1L1 cycler, this two-synodic period cycler is essentially ballistic for all launch dates. This is consistent with the findings in Ref. 13. Several three-synodic period cyclers, such as those with the prefix 5.658 as seen in Fig. 4, also exhibit relatively flat lines that hover near a $\Delta v$ of zero.

The only one-synodic period cycler investigated is cycler 6.399G1(#1), more commonly known in the literature as the Aldrin cycler. The results of the true ephemeris versions of the Aldrin cycler are seen in Fig. 3a. Remarkably, a seven-cycle propagation with a launch date of 6 August 2003 (admittedly already passed) is found that is completely ballistic. The previously published true ephemeris (outbound) solution with impulsive maneuvers had a November 1996 launch date with a total $\Delta v$ of 1.73 km/s for seven cycles.[7] Looking across all launch windows, this appears to be consistent with the magnitudes of $\Delta v$ requirements seen in Fig. 3a. The clear pattern of this extremely simple cycler is evidence that the true ephemeris geometry of the Earth and Mars does indeed repeat on the order of every 15 years (or more accurately every 32 years) as discussed in an earlier section. This previously unpublished pattern gives clear preference for the launch opportunities that reoccur every 15 years with $\Delta v$ requirements around 0.5 km/s. This repeating pattern is more difficult to identify for the two- and three-synodic cyclers because their structure is much more complicated, and the durations are two or three times longer. A similar less predictable pattern would be expected if the Aldrin cycler were also propagated for 14 or 21 synodic periods.

The Aldrin cycler is very favorable in the sense that only one vehicle is required to maintain an outbound Earth–Mars opportunity every synodic period.[7] However, it requires powered maneuvers in the circular-coplanar model because of high excess speeds at the Earth. Therefore, the discovery of a seven-cycle ballistic version of the Aldrin cycler is a significant find. Although the exact ballistic opportunity does not appear to repeat, there is a clear pattern of a preferred trajectory structure. Further investigation of this structure is an excellent candidate for future work.

Table 5 gives detailed characteristics for the minimum $\Delta v$ launch date solutions for each parent cycler documented in Figs. 3 and 4. In general, the average Earth–Mars transit times are inversely related to the excess speeds at the planets. Cycler 23 has the lowest excess speed of any solution, with an average $v_\infty$ at Earth and Mars of 4.12 and 4.79 km/s, respectively, giving an average transit time of 187 days. One of the most promising high-energy cyclers is the two-synodic period cycler 8.049gGf2 (no. 188). It requires a total $\Delta v$ of 420 m/s and has an average transit time of 95 days. The corresponding launch date is July 2042 (allowing plenty of preparation time!). The near-ballistic three-synodic period cyclers are too numerous to discuss individually. Table 5, Fig. 3, and Fig. 4 demonstrate that ballistic (or very near) three-synodic period cyclers are quite common in the accurate ephemeris model. A variety of launch dates and energy and time characteristics are available to any mission planner willing to accept that short Earth–Mars encounters only occur every three synodic periods.

If the average excess speeds before and after a flyby are not identical, either powered maneuvers are included or one of the transits is on the first or last leg. The corresponding $v_{\infty-}$ or $v_{\infty+}$ does not exist, and thus is not included in the average. This is seen more clearly in Appendix C of Ref. 19, where the full information for each transit leg is included, rather than just the averages. Also in Ref. 19, the full reproducible trajectories for each solution in Table 5 are archived. This consists of the information required to reproduce 77 full cycler trajectories. Each one corresponds to the minimum $\Delta v$ launch window for the selected parent cycler.

Table 6 gives the average $\Delta v$ over all the launch dates for each of the parent cyclers documented in Figs. 3 and 4. The entries are sorted in ascending order. This table gives a metric for the flexibility of each parent cycler with regard to launch opportunities. Impressively, there are 20 different parent cyclers that have an average cost over all 21 launch periods of less than 100 m/s per seven cycles. In some cases such as cycler 5.658Gfh+fff3(#170), there are as many as 49 legs over the course of a 45-year trajectory. It is quite remarkable that so many solutions exist that satisfy (or nearly satisfy) the constraints for each of the 48 flybys.

As expected, the general performance of an accurate ephemeris cycler is closely related to the turn ratio of the circular-coplanar parent cycler, where the turn ratio is the ratio of the maximum allowed turning angle to the maximum required turning angle. This is seen by comparing the turn ratios given in Ref. 1 with the average $\Delta v$ rankings in Table 6.

Figures 5 and 6 give two examples of full trajectory plots representative of the solutions documented in Table 5. In general, the

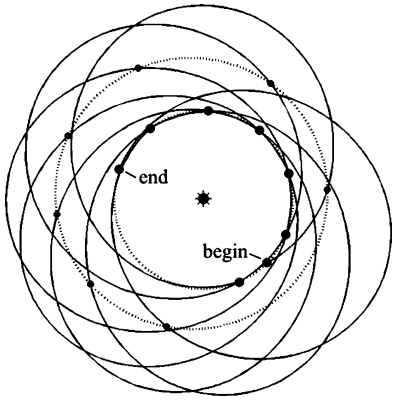


**Fig. 5 Ballistic Aldrin cycler 6.399G1(#1); launch: 6 Aug. 2003.**

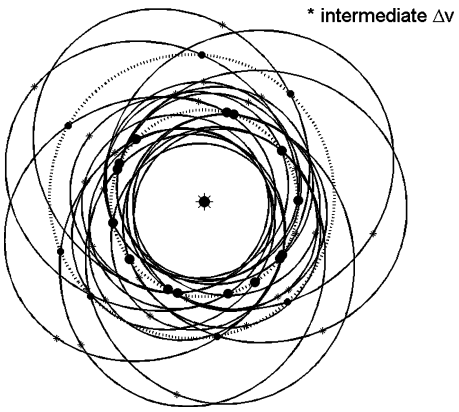


**Fig. 6 High-energy cycler 8.049gGf2(#188); launch: 26 July 2042; $\Delta v_{tot}$ = 420 m/s; avg. transit 95 days.**

**Table 5 Characteristics of smallest $\Delta v$ solutions for selected parent cyclers**

| Cycler | No. | Total $\Delta v$, m/s | Search space, sp | Launch date | Avg. E−M transit, day | Avg. $v_\infty$ E−, km/s | Avg. $v_\infty$ E+, km/s | Avg. $v_\infty$ M−, km/s | Avg. $v_\infty$ M+, km/s |
|---|---|---|---|---|---|---|---|---|---|
| 6.399G1 | 1 | 0 | 1 | Aug. 03 | 143 | 6.02 | 6.63 | 9.33 | 9.33 |
| 4.991gG2 | 83 | 0 | 11 | June 25 | 165 | 5.37 | 5.37 | 5.48 | 5.48 |
| 8.049gGf2 | 188 | 420 | 19 | July 42 | 95 | 8.65 | 8.65 | 10.34 | 10.34 |
| 8.165Gfh−f2 | 192 | 1678 | 20 | Oct. 43 | 109 | 7.78 | 7.87 | 9.96 | 9.96 |
| 8.165Gfh+f2 | 193 | 2612 | 19 | Sept. 41 | 107 | 8.02 | 8.40 | 10.01 | 10.01 |
| 9.353Gg2 | 195 | 253 | 20 | Oct. 43 | 101 | 9.12 | 9.20 | 10.73 | 10.72 |
| 3.406gGff3 | 19 | 144 | 5 | Aug. 12 | 191 | 4.92 | 4.91 | 5.12 | 5.12 |
| 3.406gfGf3 | 20 | 5 | 5 | Aug. 11 | 175 | 4.84 | 4.84 | 5.19 | 5.19 |
| 3.406gGh+fh−3 | 23 | 99 | 8 | Jan. 19 | 187 | 4.11 | 4.12 | 4.81 | 4.77 |
| 3.418gGff3 | 33 | 7 | 1 | Dec. 03 | 222 | 5.39 | 5.39 | 5.56 | 5.56 |
| 3.418gfGf3 | 34 | 20 | 20 | April 43 | 227 | 6.11 | 6.11 | 5.16 | 5.16 |
| 3.639gGf3 | 49 | 2 | 14 | Nov. 30 | 209 | 5.15 | 5.15 | 5.16 | 5.16 |
| 3.768Gh−3 | 54 | 0 | 11 | Dec. 24 | 177 | 4.70 | 5.49 | 5.25 | 5.25 |
| 3.768Gh+3 | 55 | 0 | 8 | July 18 | 183 | 4.53 | 4.99 | 4.86 | 4.86 |
| 3.768Gh−f3 | 56 | 15 | 17 | May 37 | 200 | 4.56 | 5.00 | 5.03 | 5.03 |
| 3.768Gh−fff3 | 62 | 38 | 20 | Feb. 44 | 173 | 4.37 | 5.27 | 5.19 | 5.19 |
| 3.768Gfh−ff3 | 64 | 7 | 17 | July 37 | 195 | 4.58 | 4.70 | 4.85 | 4.85 |
| 3.768Gfh+ff3 | 65 | 7 | 17 | July 37 | 195 | 4.59 | 4.74 | 4.84 | 4.84 |
| 3.784Gg3 | 74 | 74 | 1 | Aug. 03 | 176 | 4.79 | 5.29 | 4.69 | 4.69 |
| 5.125gGgf3 | 89 | 210 | 11 | July 25 | 118 | 6.33 | 6.33 | 9.64 | 9.64 |
| 5.301gGff3 | 94 | 247 | 21 | Oct. 46 | 114 | 6.48 | 6.48 | 9.59 | 9.59 |
| 5.301gGff3 | 96 | 4 | 6 | Sept. 14 | 120 | 5.81 | 5.81 | 9.46 | 9.46 |
| 5.301gGff3 | 97 | 185 | 9 | April 21 | 113 | 7.24 | 7.24 | 9.48 | 9.48 |
| 5.301ggFf3 | 98 | 272 | 16 | May 36 | 130 | 5.62 | 5.60 | 9.44 | 9.44 |
| 5.301gfGf3 | 99 | 150 | 1 | Feb. 02 | 122 | 6.05 | 6.05 | 9.28 | 9.28 |
| 5.301gFgf3 | 100 | 206 | 9 | May 21 | 114 | 7.00 | 7.00 | 9.53 | 9.53 |
| 5.301gfGff3 | 102 | 87 | 9 | April 20 | 114 | 7.22 | 7.23 | 9.46 | 9.46 |
| 5.219Ggh−3 | 111 | 0 | 16 | Aug. 35 | 119 | 5.51 | 6.20 | 9.02 | 9.02 |
| 5.219Ggh+3 | 112 | 0 | 16 | April 35 | 117 | 6.64 | 6.79 | 9.59 | 9.59 |
| 5.219Ggfh−f3 | 113 | 4 | 19 | Sept. 41 | 128 | 5.53 | 5.95 | 9.54 | 9.54 |
| 5.219Ggfh+f3 | 114 | 6 | 16 | June 35 | 124 | 5.57 | 5.58 | 9.15 | 9.15 |
| 5.225Ggg3 | 117 | 0 | 19 | Jan. 42 | 117 | 5.50 | 6.36 | 9.57 | 9.57 |
| 5.333gGf3 | 122 | 145 | 13 | June 29 | 153 | 7.74 | 7.72 | 10.09 | 10.09 |
| 5.333ggF3 | 123 | 268 | 16 | March 34 | 156 | 6.72 | 6.70 | 6.24 | 6.23 |
| 5.333gGff3 | 126 | 201 | 10 | Feb. 23 | 151 | 6.70 | 6.72 | 9.61 | 9.61 |
| 5.333gGff3 | 127 | 89 | 13 | July 29 | 154 | 7.77 | 7.76 | 10.20 | 10.20 |
| 5.333ggFf3 | 128 | 2 | 12 | July 25 | 116 | 6.42 | 6.42 | 9.68 | 9.68 |
| 5.333gfGf3 | 129 | 2 | 15 | Jan. 32 | 140 | 5.96 | 5.96 | 9.40 | 9.40 |
| 5.333gFgf3 | 130 | 272 | 21 | Sept. 46 | 149 | 6.01 | 6.02 | 9.49 | 9.49 |
| 5.333gGfff3 | 131 | 122 | 13 | July 29 | 154 | 7.78 | 7.77 | 10.20 | 10.20 |
| 5.333gfGff3 | 132 | 27 | 14 | Sept. 30 | 148 | 6.68 | 6.65 | 9.77 | 9.77 |
| 5.658Gfh−f3 | 145 | 4 | 10 | Sept. 22 | 111 | 6.91 | 6.72 | 9.57 | 9.57 |
| 5.658Gfh+f3 | 146 | 6 | 13 | Nov. 28 | 117 | 6.27 | 6.29 | 9.52 | 9.52 |
| 5.658Gfh−3 | 147 | 6 | 17 | Oct. 37 | 111 | 6.50 | 7.27 | 9.46 | 9.46 |
| 5.658gFh−3 | 148 | 30 | 15 | June 33 | 143 | 6.23 | 6.23 | 9.39 | 9.39 |
| 5.658Gfh+3 | 149 | 20 | 14 | March 31 | 114 | 6.08 | 6.37 | 9.58 | 9.58 |
| 5.658gFh+3 | 150 | 5 | 7 | May 16 | 140 | 5.96 | 6.02 | 9.42 | 9.42 |
| 5.658Gffh−3 | 151 | 15 | 14 | March 31 | 113 | 6.09 | 6.42 | 9.58 | 9.58 |
| 5.658Gffh+3 | 152 | 9 | 14 | March 31 | 113 | 6.09 | 6.42 | 9.57 | 9.57 |
| 5.658Gfh−f3 | 153 | 3 | 16 | May 35 | 120 | 6.42 | 6.36 | 9.43 | 9.43 |
| 5.658Gfh+f3 | 154 | 9 | 17 | Oct. 37 | 112 | 6.49 | 7.43 | 9.41 | 9.41 |
| 5.658Gfh−f3 | 155 | 10 | 1 | Aug. 03 | 118 | 6.75 | 7.16 | 9.44 | 9.44 |
| 5.658Gfh+f3 | 156 | 9 | 1 | July 03 | 118 | 6.74 | 7.05 | 9.44 | 9.44 |
| 5.658Gfh−ff3 | 157 | 15 | 17 | Oct. 37 | 112 | 6.50 | 6.96 | 9.43 | 9.43 |
| 5.658Gfh+ff3 | 158 | 11 | 7 | April 16 | 109 | 6.51 | 6.65 | 9.57 | 9.57 |
| 5.658Gfh−ff3 | 159 | 7 | 21 | March 46 | 119 | 6.25 | 6.71 | 9.55 | 9.55 |
| 5.658gfh−fFzero3 | 160 | 7 | 2 | July 05 | 113 | 6.25 | 6.25 | 9.74 | 9.74 |
| 5.658gfh−fFpi3 | 161 | 47 | 11 | July 24 | 146 | 6.74 | 6.76 | 10.14 | 10.14 |
| 5.658Gfh+ff3 | 162 | 11 | 10 | Nov. 22 | 118 | 6.84 | 7.48 | 9.63 | 9.63 |
| 5.658gfh+fFzero3 | 163 | 10 | 17 | Aug. 37 | 110 | 6.52 | 6.52 | 9.85 | 9.85 |
| 5.658gfh+fFpi3 | 164 | 271 | 7 | Jan. 16 | 148 | 6.80 | 6.68 | 9.82 | 9.82 |
| 5.658Gfh−ff3 | 165 | 27 | 21 | March 46 | 113 | 6.05 | 6.38 | 9.45 | 9.45 |
| 5.658Gfh−ff3 | 166 | 5 | 20 | Nov. 43 | 119 | 6.10 | 6.17 | 9.57 | 9.57 |
| 5.658Gfh+ff3 | 167 | 9 | 17 | Sept. 37 | 115 | 6.47 | 6.39 | 9.42 | 9.42 |
| 5.658Gfh+ff3 | 168 | 9 | 14 | March 31 | 113 | 6.07 | 6.64 | 9.47 | 9.47 |
| 5.658Gfh−fff3 | 169 | 14 | 17 | Oct. 37 | 112 | 6.52 | 7.31 | 9.42 | 9.42 |
| 5.658Gfh+fff3 | 170 | 9 | 10 | Nov. 22 | 118 | 6.83 | 7.50 | 9.62 | 9.62 |
| 5.658Gffh−ff3 | 171 | 15 | 13 | Feb. 29 | 119 | 6.44 | 7.15 | 9.65 | 9.66 |
| 5.658Gffh+ff3 | 172 | 10 | 4 | Nov. 09 | 110 | 6.68 | 6.63 | 9.79 | 9.79 |
| 5.679Gfh−f3 | 175 | 8 | 7 | March 16 | 111 | 6.52 | 6.40 | 9.61 | 9.61 |
| 5.679Gfh+f3 | 176 | 6 | 16 | June 35 | 113 | 6.58 | 6.44 | 9.43 | 9.43 |
| 5.751Ggf3 | 177 | 1 | 3 | Nov. 07 | 113 | 7.03 | 7.33 | 9.78 | 9.78 |
| 5.751ggF3 | 178 | 0 | 9 | Sept. 20 | 108 | 7.39 | 7.39 | 9.96 | 9.96 |
| 5.751Ggff3 | 179 | 3 | 19 | Dec. 41 | 113 | 6.82 | 7.33 | 9.90 | 9.90 |
| 5.751Gfgf3 | 180 | 5 | 17 | Oct. 37 | 109 | 6.93 | 7.35 | 9.56 | 9.56 |
| 6.205gG3 | 184 | 51 | 20 | Sept. 42 | 220 | 6.50 | 6.51 | 6.20 | 6.20 |
| 7.954Gg3 | 189 | 239 | 19 | Oct. 41 | 131 | 8.26 | 7.77 | 6.71 | 6.71 |

**Table 6 Solutions sorted by average $\Delta v$ over all of the launch dates**

| Parent cycler | No. | Avg. tot. $\Delta v$, m/s |
|---|---|---|
| 5.658Gfh+ff3 | 162 | 24 |
| 5.658Gfh−f3 | 155 | 28 |
| 4.991gG2 | 83 | 29 |
| 5.658Gfh+ff3 | 158 | 30 |
| 5.658Gfh+f3 | 156 | 37 |
| 5.658Gfh−ff3 | 157 | 37 |
| 5.658Gfh−ff3 | 159 | 37 |
| 5.658Gfh+fff3 | 170 | 41 |
| 5.658Gfh−fff3 | 169 | 41 |
| 5.658Gffh+ff3 | 172 | 61 |
| 5.658Gffh−ff3 | 171 | 65 |
| 5.658Gfh+ff3 | 168 | 69 |
| 5.679Gfh+f3 | 176 | 74 |
| 5.333gfGf3 | 129 | 75 |
| 5.658Gfh−f3 | 145 | 82 |
| 5.658Gfh−ff3 | 166 | 82 |
| 5.751Ggf3 | 177 | 88 |
| 5.219Ggfh+f3 | 114 | 91 |
| 5.679Gfh−f3 | 175 | 95 |
| 5.658Gfh+f3 | 146 | 100 |
| 5.658Gfh−3 | 147 | 106 |
| 5.658Gfh−ff3 | 165 | 106 |
| 5.219Ggfh−f3 | 113 | 108 |
| 5.219Ggh+3 | 112 | 122 |
| 3.768Gfh+ff3 | 65 | 126 |
| 5.658gfh+fFzero3 | 163 | 129 |
| 5.658gfh−fFzero3 | 160 | 131 |
| 5.658Gfh+ff3 | 167 | 140 |
| 5.219Ggh−3 | 111 | 141 |
| 5.301gGff3 | 96 | 141 |
| 5.751Ggff3 | 179 | 148 |
| 3.768Gfh−ff3 | 64 | 153 |
| 5.225Ggg3 | 117 | 158 |
| 3.639gGf3 | 49 | 161 |
| 5.658Gffh−3 | 151 | 166 |
| 5.658Gfh+3 | 149 | 174 |
| 5.658Gffh+3 | 152 | 180 |
| 5.658Gfh−f3 | 153 | 207 |
| 5.658Gfh+f3 | 154 | 214 |
| 5.751Gfgf3 | 180 | 238 |
| 5.751ggF3 | 178 | 273 |
| 6.205gG3 | 184 | 315 |
| 5.301gFgf3 | 100 | 346 |
| 5.125gGgf3 | 89 | 361 |
| 5.658gFh+3 | 150 | 382 |
| 5.301gGff3 | 97 | 393 |
| 5.333ggFf3 | 128 | 394 |
| 5.333gfGff3 | 132 | 403 |
| 5.658gFh−3 | 148 | 411 |
| 3.768Gh−fff3 | 62 | 428 |
| 5.333gGff3 | 127 | 455 |
| 5.301gfGf3 | 99 | 469 |
| 3.418gfGf3 | 34 | 507 |
| 3.418gGff3 | 33 | 526 |
| 7.954Gg3 | 189 | 536 |
| 3.768Gh−3 | 54 | 544 |
| 3.768Gh+3 | 55 | 551 |
| 5.333gGff3 | 126 | 595 |
| 3.768Gh−f3 | 56 | 597 |
| 5.301ggFf3 | 98 | 687 |
| 5.301gGff3 | 94 | 709 |
| 9.353Gg2 | 195 | 714 |
| 5.333gFgf3 | 130 | 720 |
| 5.301gfGff3 | 102 | 732 |
| 8.049gGf2 | 188 | 818 |
| 5.333gGfff3 | 131 | 823 |
| 3.784Gg3 | 74 | 869 |
| 5.333gGf3 | 122 | 871 |
| 3.406gGff3 | 19 | 942 |
| 3.406gfGf3 | 20 | 992 |
| 5.333ggF3 | 123 | 1176 |
| 5.658gfh−fFpi3 | 161 | 1430 |
| 5.658gfh+fFpi3 | 164 | 1752 |
| 3.406gGh+fh−3 | 23 | 2181 |
| 8.165Gfh−f2 | 192 | 2471 |
| 6.399G1 | 1 | 3297 |
| 8.165Gfh+f2 | 193 | 3612 |

trajectories are difficult to visualize because of the typical complexity and duration. The example trajectories presented are two of the simplest. The first one is the seven-cycle ballistic propagation of the Aldrin cycler, and the second is one of the promising high-energy two-synodic period cyclers.

In Fig. 5, note that the trajectory begins and ends almost on opposing sides of the sun. Initially, seven cycles of the idealized cycler have a total duration very near the 15-year approximate inertial repeat time of Earth and Mars. Because this total duration is not fixed in the optimization procedure, the solution is free to change as necessary. In most cases, the total duration remains in the neighborhood of the original, thus increasing the likelihood that the general pattern is repeatable. However, as seen in Fig. 5, there are times when the optimizer arrives at a much lower cost by departing from the original total duration. Although these patterns are less likely to be repeatable, it was decided for the broad purposes of this survey to favor the lowest cost cyclers instead.

## Most Promising Cyclers

Because only one interplanetary transit leg is guaranteed each cycle, the one- and two-synodic period cyclers are clearly favorable over the three- or more synodic period cyclers. Therefore, it is generally recommended that future work focuses on these solutions. The S1L1 cycler (4.991Gg2), 8.049gGf2, and the Aldrin cycler (6.399G1) debatably have the most promising characteristics. Further optimization of these and the other two-synodic period cyclers documented in Refs. 1 and 3 is suggested.

## Conclusions

A robust and efficient method is presented to optimize long-duration ballistic trajectories with multiple flybys. Analytic gradients are derived, and postprocessed intermediate maneuvers are optimized to ensure position continuity. The method is applied to a continuation algorithm developed to walk several cycles of existing circular-coplanar cycler solutions toward analogous accurate ephemeris solutions. The algorithm is then applied to 203 promising circular-coplanar parent cyclers for a variety of launch windows. Three main conclusions are drawn.

First, efficiency is the main driver in the development of the constraint function and the parameter vector. The resulting system, complete with analytic gradients, is a stand-alone system that could prove useful in the preliminary design of any long-duration, multiple-flyby, ballistic, patched conic trajectory.

Second, the continuation algorithm demonstrates the feasibility of transitioning simple model solutions to accurate ephemeris solutions. Again, the method is applied to several cycles of Earth–Mars cyclers, but could be applied to any similar class trajectory with a known idealized solution.

Finally, and most importantly, this study demonstrates the existence of hundreds of ephemeris model ballistic cyclers. It is a broad survey of ephemeris cyclers that originate from the general class of idealized cyclers that are composed of Earth to Earth free returns. Although several intermediate steps are necessary, such as finding solutions in an idealized model, the ultimate goal of cycler trajectory research, in general, is to obtain flyable cycler trajectories. Although the solutions presented in this study are still subject to approximations, such as Keplerian motion, and the zero-sphere-of-influence flybys, the next step of using the most accurate model possible is expected to be minor compared to the step demonstrated here. The solutions documented conservatively represent at least an order-of-magnitude increase in the number of known accurate ephemeris cycler trajectories. Many solutions have ballistic (or near-ballistic) launch opportunities every synodic period.

In addition to removing the mentioned assumptions, extensions from this work include further customized optimization of individual solutions, such as the Aldrin cycler and the two-synodic period cyclers. On a larger scale, the basic problem could be reformulated to define new classes of cyclers, such as those that incorporate Venus and or Mars flybys in the original idealized model.

## Acknowledgments

The research described in this paper was carried out at the University of Texas at Austin and was partially supported by a Graduate Student Researchers Program Fellowship from NASA's Goddard Space Flight Center.

## References

[1]Russell, R., and Ocampo, C., "Global Search for Idealized Free-Return Earth–Mars Cyclers," *Journal of Guidance, Control, and Dynamics*, Vol. 28, No. 2, 2005, pp. 194–208.

[2]McConaghy, T. T., Russell, R. P., and Longuski, J. M., "Towards a Standard Nomenclature for Earth–Mars Cycler Trajectories," *Journal of Spacecraft and Rockets*, Vol. 42, No. 4, 2005, pp. 694–698.

[3]Russell, R. P., and Ocampo, C. A., "Systematic Method for Constructing Earth–Mars Cyclers Using Free-Return Trajectories," *Journal of Guidance, Control, and Dynamics*, Vol. 27, No. 3, 2004, pp. 321–335.

[4]McConaghy, T. T., Longuski, J. M., and Byrnes, D. V., "Analysis of a Broad Class of Earth–Mars Cycler Trajectories," *Journal of Spacecraft and Rockets*, Vol. 41, No. 4, 2004, pp. 622–628.

[5]Byrnes, D. V., McConaghy, T. T., and Longuski, J. M., "Analysis of Various Two Synodic Period Earth–Mars Cycler Trajectories," AIAA Paper 2002-4423, Aug. 2002.

[6]McConaghy, T. T., Yam, C. H., Landau, D. F., and Longuski, J. M., "Two-Synodic-Period Earth–Mars Cyclers with Intermediate Earth Encounter," American Astronautical Society, Paper 03-509, Aug. 2003.

[7]Byrnes, D. V., Longuski, J. M., and Aldrin, B., "Cycler Orbit Between Earth and Mars," *Journal of Spacecraft and Rockets*, Vol. 30, No. 3, 1993, pp. 334–336.

[8]Rall, C. S., "Freefall Periodic Orbits Connecting Earth and Mars," Ph.D. Dissertation, Dept. of Aeronautics and Astronautics, Massachusetts Inst. of Technology, Cambridge, Oct. 1969.

[9]Menning, M. D., "Freefall Periodic Orbits Connecting Earth and Venus," M.S. Thesis, Dept. of Aeronautics and Astronautics, Massachusetts Inst. of Technology, Cambridge, July 1968.

[10]Hollister, W. M., "Periodic Orbits for Interplanetary Flight," *Journal of Spacecraft and Rockets*, Vol. 6, No. 4, 1969, pp. 366–369.

[11]Niehoff, J., "Pathways to Mars: New Trajectory Opportunities," American Astronautical Society, Paper 86-172, July 1986.

[12]Chen, K., McConaghy, T., Okutsu, M., and Longuski, J., "A Low-Thrust Version of the Aldrin Cycler," AIAA Paper 2002-4421, Aug. 2002.

[13]McConaghy, T. T., Yam, C. H., Landau, D. F., and Longuski, J. M., "Two-Synodic-Period Earth–Mars Cyclers with Intermediate Earth Encounter," American Astronautical Society, Paper 03-509, Aug. 2003.

[14]McConaghy, T. T., Chen, J. C., Landau, D. F., and Longuski, J. M., "A Powered Earth–Mars Cycler with Three Synodic-Period Repeat Time," American Astronautical Society, Paper 03-510, Aug. 2003.

[15]Stevens, R., and Ross, M., "Preliminary Design of Earth–Mars Cyclers Using Solar Sails," American Astronautical Society, Paper 03-244, Feb. 2003.

[16]Landau, D., and Longuski, J., "Comparative Assessment of Human Missions to Mars," American Astronautical Society, Paper 03-513, Aug. 2003.

[17]Chen, K. J., Landau, D. F., McConaghy, T. T., Okutsu, M., Longuski, J. M., and Aldrin, B., "Preliminary Analysis and Design of Powered Earth–Mars Cycling Trajectories," AIAA Paper 2002-4422, Aug. 2002.

[18]Rauwolf, G., A., and Friedlander, A., L., "A Mars Cycler Architecture Utilizing Low-Thrust Propulsion," AIAA Paper 2002-5046, Aug. 2002.

[19]Russell, R. P., "Global Search and Optimization for Free-Return Earth–Mars Cyclers," Ph.D. Dissertation, Dept. of Aerospace Engineering and Engineering Mechanics, The Univ. of Texas at Austin, Aug. 2004.

[20]Standish, E. M., "JPL Planetary and Lunar Ephemerides" [CD-ROM], Willman-Bell, Inc., Richmond, VA, 1997.

[21]Seidelmann, K. P. (ed.), *Explanatory Supplement to the Astronomical Almanac*, University Science Books, Mill Valley, CA, 1992, p. 704.

[22]Betts, J. H., "Survey of Numerical Methods for Trajectory Optimization," *Journal of Guidance, Control, and Dynamics*, Vol. 21, No. 2, 1998, pp. 193–207.

[23]Russell, R., and Ocampo, C., "A Geometric Analysis of Free-Return Trajectories Following a Gravity-Assisted Flyby," *Journal of Spacecraft and Rockets*, Vol. 42, No. 1, 2005, pp. 694–698.

[24]Goldberg, D. E., *Genetic Algorithms in Search, Optimization, and Machine Learning*, Addison Wesley Longman, Reading, MA, 1989.

[25]Rogata, P., Di Sotto, E., Granziano, M., and Graziani, F., "Guess Value for Interplanetary Transfer Through Genetic Algorithms," American Astronautical Society, Paper 03-140, Feb. 2003.

[26]Vasile, M., "A Global Approach to Optimal Space Trajectory Design," American Astronautical Society, Paper 03-141, Feb. 2003.

[27]Gill, P. E., Murray, W., and Saunders, M. A., "SNOPT: An SQP Algorithm for Large Scale Constrained Optimization," *SIAM Journal of Optimization*, Vol. 12, No. 4, 2002, pp. 979–1006.

[28]Hull, D. G., and Williamson, W. E., "Numerical Derivatives for Parameter Optimization (Applied to Drag Coefficient Interpolation)," *Journal of Guidance and Control*, Vol. 2, No. 2, 1979, pp. 158–160.

[29]Zimmer, S., and Ocampo, C. A., "Combined Long Duration Burns and Gravity Assist Trajectories Using Analytical Gradients," American Astronautical Society, Paper 03-576, Aug. 2003.

[30]Montenbruck, O., and Gill, E., *Satellite Orbits*, Berlin, Springer-Verlag, 2000, Chap. 7.

[31]Broucke, R. A., and Cefola, P. J., "On the Equinoctial Orbit Elements," *Celestial Mechanics*, Vol. 5, No. 3, 1972, pp. 303–310.

[32]Dow, J. M., "Non-Singular Partial Derivatives for Synchronous Orbits," European Space Operations Centre, Orbit and Attitude Div., Working Paper 22, Darmstadt, Germany, May 1975.

[33]Byrnes, D. V., and Bright, L. E., "Design of High-Accuracy Multiple-Flyby Trajectories Using Constrained Optimization," American Astronautical Society, Paper 95-307, Feb. 1995.

[34]Sauer, C. G., "MIDAS: Mission Design and Analysis Software for the Optimization of Ballistic Interplanetary Trajectories," *Journal of the Astronautical Sciences*, Vol. 37, July–Sept. 1989, pp. 251–259.

[35]Ocampo, C. A., "An Architecture for a Generalized Spacecraft Trajectory Design and Optimization System," *Libration Point Orbits and Applications: Proceedings of the Conference Aiguablava, Spain 10–14 June 2002*, edited by J. J. Masdemont, M. W. Lo, and G. Gómez, World Scientific, River Edge, NJ, 2003, pp. 529–571.